DEVELOPMENT OF AN EXPERIMENTAL FACILITY FOR FLAME SPEED MEASUREMENTS IN POWDERED AEROSOLS

A Thesis

by

ANDREW JOHN VISSOTSKI

Submitted to the Office of Graduate Studies of
Texas A&M University
in partial fulfillment of the requirements for the degree of

MASTER OF SCIENCE

August 2012

Major Subject: Mechanical Engineering

Development of an Experimental Facility for Flame Speed Measurements in Powdered Aerosols

DEVELOPMENT OF AN EXPERIMENTAL FACILITY FOR FLAME SPEED MEASUREMENTS IN POWDERED AEROSOLS

A Thesis

by

ANDREW JOHN VISSOTSKI

Submitted to the Office of Graduate Studies of
Texas A&M University
in partial fulfillment of the requirements for the degree of

MASTER OF SCIENCE

Approved by:

Co-Chairs of Committee,	Eric L. Petersen
	Mahboobul Mannan
Committee Member,	David Staack
Head of Department,	Jerry Caton

August 2012

Major Subject: Mechanical Engineering

ABSTRACT

Development of an Experimental Facility for Flame Speed Measurements in Powdered Aerosols.

(August 2012)

Andrew John Vissotski, B.S., Boise State University

Co-Chairs of Advisory Committee: Dr. Eric L. Petersen
Dr. Mahboobul Mannan

Research with heterogeneous mixtures involving solid particulate in closed, constant-volume bombs is typically limited by the powder dispersion technique. This work details the development of an experimental apparatus that promotes ideal conditions, namely a quiescent atmosphere and uniform particle distribution, for measuring laminar, heterogeneous flame propagation. In this thesis, two methods of dispersing particles are investigated. In the first, heterogeneous mixtures are made in a secondary vessel that is connected to the main experiment. Particles are dispersed into the secondary vessel by adapting a piston-driven particle injector, which has been shown to produce uniform particle distributions. The heterogeneous mixture is then transferred to the main bomb facility and ignited after laminar conditions are achieved. In the second method of dispersion, particles are directly injected into the main experimental facility using a strong blast of compressed air. As with the first approach, enough time is given (~4 minutes) for the mixture to become quiescent before ignition occurs. An extinction diagnostic is also applied to the secondary mixing vessel as well as the primary experimental facility (for both dispersion methods) to provide a qualitative understanding of the dispersion technique. To perform this diagnostic a 632.8-nm, 5-mW Helium-Neon (HeNe) laser was employed. Aluminum nano-particles with an average diameter of 100 nm were used in this study. It was found that for typical dust loadings produced with both dispersion techniques, a pure dust-air system would not ignite due to the current spark ignition system. Thus, a hybrid mixture of $Al/CH_4/O_2/N_2$ was employed to achieve the project goal of demonstrating a system for controlled laminar flame speed measurements in aerosol mixtures. With the hybrid mixture, the combustion characteristics were studied both with and without the presence of nano-

Al particles. Based on the experimental results, the simplicity of the “direct-injection” methodology compared to that of the “side-vessel” is desirable and will be further investigated as a viable alternative, or improvement, to the side-vessel technology.

ACKNOWLEDGMENTS

First and foremost, I would like to acknowledge my advisor, Dr. Eric Petersen. His work ethic and dedication to his students is above the call of duty and merits recognition. I strongly feel this work would not have been achievable without his guidance. Thanks also go out to my committee co-chair and committee member, Dr. Mahboobul 'Sam' Mannan and Dr. David Staack, respectively. I also recognize Dr. Zhengdong Cheng for substituting during the oral exam for Dr. Mannan. In addition, I would also like to acknowledge the financial support from the Mary Kay O'Connor Process Safety Center at Texas A&M University used to fund this project.

I also thank my colleagues, past and present, for the support they have shown me throughout the completion of this work. I thank Alejandro Camou for his patience and tireless efforts in assisting with the experiments performed herein. This work would not have been possible without your contributions. I also thank Michael Krejci for helpful discussions during the design and fabrication phases of the project.

I would also like to recognize my undergraduate advisor, Dr. Don Plumlee at Boise State University, for inspiring me to pursue an advanced degree. I finally thank my family for their endless care and encouragement. I especially thank my mother for all the sacrifices she has made in support of my education.

NOMENCLATURE

Abbreviations

A	Area (cm^2)
AMV	Aerosol Mixing Vessel
C	Extinction Cross Section (cm^2)
d	Particle Diameter (nm)
H	Enthalpy (kJ)
I	Laser Intensity (W/m^2)
LDA	Laser Doppler Anemometry
N	Particle Number Density (# of particles/cm^3)
NFPA	National Fire Protection Agency
P	Pressure (atm)
PIV	Particle Image Velocimetry
Q	Extinction Efficiency
R	Flame Radius (cm)
S	Flame Speed (cm/s)
T	Temperature (K)
t	Time (s)
U	Internal Energy (kJ)
U.S. CSB	United States Chemical Safety and Hazard Investigation Board
V	Volume (m^3)

Subscripts

abs	Absorption
AF	Adiabatic Flame
b	Burned condition

ext	Extinction
L	Laminar flame
m	Markstein
sca	Scattering
u	Unburned condition
o	Incident

Superscripts

o	Un-stretched condition

Greek Symbols

α	Flame stretch (1/s)
σ	Extinction Coefficient (1/cm)
τ	Optical Depth

TABLE OF CONTENTS

LIST OF FIGURES

Page

Page

Page

LIST OF TABLES

CHAPTER I

INTRODUCTION

Dust explosions in the process industries have been a prevalent danger for many years. The onset of the industrial revolution has increased the frequency of occurrences tremendously with food, wood, metals, and plastics being the most common. As such, there is a large need and motivation to study the dust explosion phenomenon in an attempt to properly design safety equipment to protect and prevent accidental explosions from happening. Experimental research involving combustible dusts is conducted in a wide range of facilities, but is most commonly performed in constant-volume vessels. Dynamic pressure data are collected using these bomb facilities, and optical access is often very limited. These data are typically vessel dependent, whereas for the present study a more fundamental parameter space is sought.

The focus and interest in this work is to obtain a better understanding of the physics and chemical kinetics associated with laminar flame propagation in heterogeneous mixtures. Experimental data gathered from each test are used to calculate the laminar flame speed, or burning velocity, which is a fundamental parameter of the reacting mixture that can then be used to improve kinetics and particle burning models and provide the necessary information for designing safety equipment. To this end, the existing flame speed bomb located at Texas A&M University has been modified to accommodate powdered aerosols in a repeatable, controlled way. Two methods are investigated in this work. The first involves a separate side-vessel methodology and the second utilizes a simpler, direct-injection technique.

In the "side-vessel" methodology, heterogeneous mixtures involving solid particulate are made in a secondary vessel and transferred to the experimental apparatus. A key element of the side-vessel technique is that larger particles and agglomerates will settle to the bottom of the vessel. When the heterogeneous mixture is transferred into the flame speed bomb, only particles of a certain size-range that have not settled to the bottom are present in the experimental facility. Once ignited, a spherical flame

---

This thesis follows the style of *Combustion Science and Technology*.

expands outward from this central location and can be monitored through optical ports located at each end of the cylindrical flame speed vessel. With the “direct injection” technique, a mass of particles is loaded into a container and dispersed directly into the flame speed bomb with a strong blast of compressed air. As with the “side-vessel” approach, the mixture is allowed to become quiescent before ignition occurs.

From such an experiment comes the laminar flame speed, or burning velocity, which is a fundamental parameter of the reactive mixture and does not depend of the geometry of the equipment. This thesis describes the methodology and characterization of a facility that can provide repeatable laminar flame speed measurements in an aerosol-laden fuel-oxidizer mixture.

This thesis is divided by chapters. In Chapter II, the background of dust explosions is discussed, including the history of dust explosions in the process industries, two case studies from accidental explosions involving combustible dusts, a discussion of flame propagation in heterogeneous mixtures, measurement techniques used throughout the literature in dust explosion research, and a closer look at research with constant-volume bombs. Chapter III goes over the experimental facility and approach. In this chapter, details of the current experimental apparatus used for taking the flame speed measurements for homogeneous vapor phase mixtures of fuel and oxidizer are discussed. The project goals are outlined, and the powder injection approach is explained, along with details associated with additional equipment required to make heterogeneous mixtures. Initial results are covered in Chapter IV, describing the experimental parameters chosen to investigate flame speed measurements using a hybrid mixture of $Al/CH_4/O_2/N_2$. Experimental flame images are also presented in Chapter IV and compared to similar cases without aluminum particles, which are captured using a high-speed camera. Chapter V concludes this thesis.

CHAPTER II

BACKGROUND

History of Dust Explosions

Dust explosions are a serious safety concern in the process industries and have been for hundreds of years. The first documented dust explosion occurred on December 14, 1785 in Turin, Italy (Eckhoff, 2003). According to historical records, a violent explosion occurred in a dry-flour storage facility and was thought to be the result of a dust cloud contacting the flame of a lamp. The explosion spread quickly throughout the facility, and the sudden pressure rise caused the windows to blow out of their frames. An extremely loud noise was heard for a considerable distance, and a very bright flame, which lasted only a few seconds, was seen at the facility. During the 150-200 years that have passed since this event, the expanding chemical and metallurgical industries have established a steadily increasing number of new, finely divided combustible solids (Eckhoff, 2009). Consequently, dust explosion accidents have also experienced a steady increase in occurrences.

Between 1980 and 2005, at least 281 combustible dust-related fires and explosions took place in the United States (U.S. CSB, 2006). It is worthy to note that numerous other dust explosion events have taken place throughout the other parts of the world as well, particularly in Europe. The statistics presented in this section are only regarding events in the United States. Over this span of twenty-five years, a total of 119 fatalities and 718 injuries occurred in addition to millions of dollars in extensive damage to the industrial facilities and loss of productivity. People involved in such catastrophic events are often either burned by the intense heat from the flame propagating in the dust-air mixture or are struck by flying objects or falling structures.

A wide range of materials used in process industries are capable of producing disastrous dust explosions. These events can occur in any industry that handles combustible dusts, including but not limited to metal fabrication, plastics, furniture/wood products, chemical manufacturing, and food products (U.S. CSB, 2006). The pie chart in Figure 1 shows the statistical distribution of dust types involved in the

281 events taking place from 1980 to 2005. As shown in Fig. 1, wood- and food-related products incorporate the majority of explosion/disaster events by a combined measure of nearly 50%. Metal dusts also make a significant contribution to the overall frequency of dust explosions. Together, all three of these dust types account for more than 60% of all explosions that occurred during this timeframe. Plastics are also of importance, contributing to 14% of the total number of events, while Coal, Inorganics, and other dusts have the least number of occurrences.

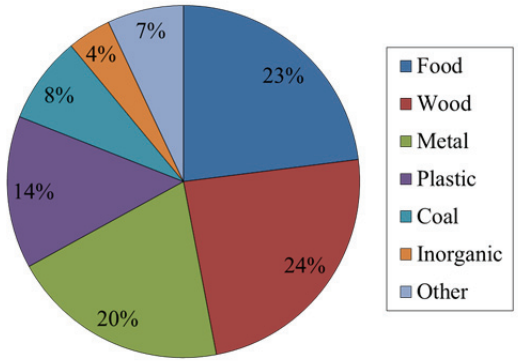

Figure 1 Combustible dust incidents by material from 1980-2005 (U.S. CSB, 2006).

The following case studies are meant to illustrate the severity of a dust explosion and the need to understand them through basic research. Catastrophic events such as these could have been mitigated or possibly prevented if sufficient information were known about the dust explosion phenomena. Experimental data can be used to adapt safety precautions and design safety equipment, such as fast-acting vents or extinguishing systems.

Case Study 1: West Pharmaceutical Services, Inc.

A massive dust explosion involving the West Pharmaceutical Services facility in Kinston, North Carolina occurred on January 29, 2003 (U.S. CSB, 2004). The explosion killed six people, injured at least 38 others, and destroyed the facility. The aftermath of the dust explosion involving the Kinston plant is shown in Figure 2.

This particular factory produced rubber plungers for syringes used in the pharmaceutical industry. The part of the facility involved in the dust explosion was used to compound the rubber used in the plungers. Part of the compounding process involved freshly milled rubber strips dipped into a solution of polyethylene, water, and a surfactant to cool the material. As the rubber dried, very fine particles of polyethylene were carried by convective currents within the facility and settled on surfaces above the suspended ceiling. Although ground-level work areas were kept extremely clean, few employees were aware of the dust accumulation above. In addition, the Materials Safety Data Sheet (MSDS) on-hand for polyethylene did not list the material as an explosion hazard for certain conditions.

The built-up dust became dispersed in the production area by some unknown means of disturbance. Because of the extent of damage to the Kinston facility, it was not possible to identify what event caused the dust to become dispersed or what ignited it (U.S. CSB, 2004). However, the electrical system in the vicinity was not rated for compatibility with combustible dusts and is believed to be the most likely source of ignition. The U.S. CSB determined that the explosion could have been prevented or controlled if West Pharmaceuticals had adhered to the NFPA standard 654 (NFPA, 2000). This standard specifies that areas not easily accessed for cleaning, such as the ceiling area above the production facility, should be sealed to prevent potential accumulation of explosive dusts.

Figure 2 West Pharmaceutical Services facility in Kinston, North Carolina after dust explosion incident involving polyethylene powder. Image from U.S. CSB (2004).

Case Study 2: Imperial Sugar Processing Facility

Another, more recent, substantial dust explosion involving highly explosive sugar dust at an Imperial Sugar manufacturing facility in Port Wentworth, Georgia on February 7, 2008 (U.S. CSB, 2009). The tragic event resulted in 14 fatalities. Eight workers died on-site, and the six others eventually passed away from their injuries at a hospital. In addition to the fatalities, 36 other workers were treated for serious burns and injuries. The explosion completely demolished the sugar packing buildings, palletizer room, and storage silos, shown in Figure 3.

The facility at Port Wentworth housed a refinery that converts raw sugar cane into granulated sugar. A system of screw and belt conveyors was used to transport granulated sugar from the refinery to the storage silos. Another system of conveyor belts was then used to transport the granulated sugar from the silos to specialty sugar processing areas and packaging machines. The company installed steel panels over the conveyor belt system completely encapsulating it in an effort to reduce the amount of sugar dust building up on factory surfaces. However, this enclosed volume allowed the buildup of explosive concentrations of sugar dust. It is believed by the U.S. CSB that the first explosion initiated in this confined space by an unknown ignition source (U.S. CSB, 2009). The pressure wave from the explosion propagated throughout the rest of the factory causing sugar dust that had accumulated on floors and elevated surfaces to become dispersed in the air. Subsequent explosions were allowed to propagate through the newly dispersed sugar dust. Concrete floors were moved by the pressure waves and brick walls were collapsed.

Over the years, the sugar-processing facility experienced several fires involving granulated and powdered sugars. However, the company management and workers did not recognize the significant safety hazard associated with the sugar dust, despite the previous encounters. The U.S. CSB recognized that initial explosions would likely not have occurred if Imperial Sugar had equipped the steel conveyor belt enclosure with explosion vents to safely vent the rapid buildup of pressure from a confined dust

explosion (U.S. CSB, 2009). It also suggests the secondary explosion could have been prevented if better housekeeping practices were implemented.

Figure 3 Imperial Sugar factory in Port Wentworth, Georgia after a dust explosion incident involving massive accumulations of highly combustible sugar dust throughout the packaging building. Image from U.S. CSB (2009).

Flame Propagation in Heterogeneous Mixtures

Any solid material that can burn in air will do so with a certain rate that increases as the material is divided into smaller portions while keeping the same total volume (Eckhoff, 2003). For example, by decreasing the size of the combustible solid, the surface area-to-volume ratio increases, along with the rate of combustion. This concept is illustrated with organic wood material in Figure 4. A large log of wood (Figure 4a), once ignited, will burn slowly and release energy in the form of heat over a long period of time. If the same log were divided into smaller pieces (Figure 4b) and ignited, the rate of combustion is increased. This increased rate can be attributed to the larger amount of surface area contacting the oxidizer. If the wood pieces were divided into even smaller pieces (Figure 4c), say on the order of 0.1 mm or less and were suspended into a sufficient volume of oxidizer, such as air, to give each particle ample space for unobstructed burning, the combustion rate is much faster than the previous cases and the energy is released rapidly rather than over a long period of time. This circumstance is referred to as a dust explosion.

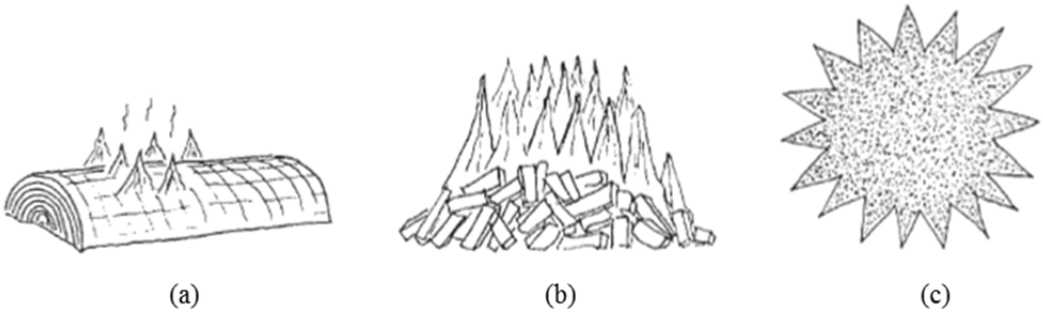

Figure 4 Illustration of how solid material subdivision increases burning rate. (a) Slow burning, (b) Fast combustion, (c) Dust explosion. Image from Eckhoff, 2003.

The three requirements for combustion are a fuel, an oxidizer, and an adequate heat or ignition source (Cashdollar, 2000). These three items are commonly referred to as the "fire triangle". Fuel, in this case, can be any material capable of producing a rapid, exothermic reaction with the oxidizing material. For this particular case the fuel is a combustible dust. However, for a dust explosion to occur, the fire triangle must be expanded to incorporate two additional elements: dispersion and confinement. This is shown in Figure 5 as the "dust explosion pentagon". A dust explosion can only occur when the combustible dust is dispersed in the oxidizer (usually air) at the same time the ignition source (heat) is applied. The confinement is necessary because the energy released from the burning dust will drastically raise the pressure within the volume, often leading to failure of enclosure.

Figure 5 Classic "fire triangle" (left) and "dust explosion pentagon" (right).

A dust explosion is, in its most basic form, a flame front propagating through the dust-air mixture. Analogies can be drawn between the heterogeneous systems and the traditional homogenous,

premixed case (Proust and Veyssiere, 1988). Consider a region of space, of fixed area, initially filled with a fuel and oxidizer referred to in Figure 6 as reactants. If the mixture is ignited by some means, a planar flame will form and propagate in one direction through the reactants creating products in its wake. The speed at which this flame propagates is referred to as the laminar flame speed, S_L, and is a fundamental property of the mixture. In general, the flame speed is a function of the mixture stoichiometry, reactant species, as well as initial conditions, such as pressure and temperature (Law, 2006). Much work has been done to analyze and understand the laminar flame speed of homogeneous mixtures in the vapor phase. The same methodology can be applied to heterogeneous mixtures of solid particulate as the fuel and air as the oxidizer, as shown in Figure 6. Igniting the mixture by some means will still result in a flame front propagating from left to right as shown in the figure. The speed at which the flame travels will also be a function of the mixture stoichiometry, reactivity, and initial conditions. However, the most applicable initial condition for a dust-air system is standard temperature and pressure.

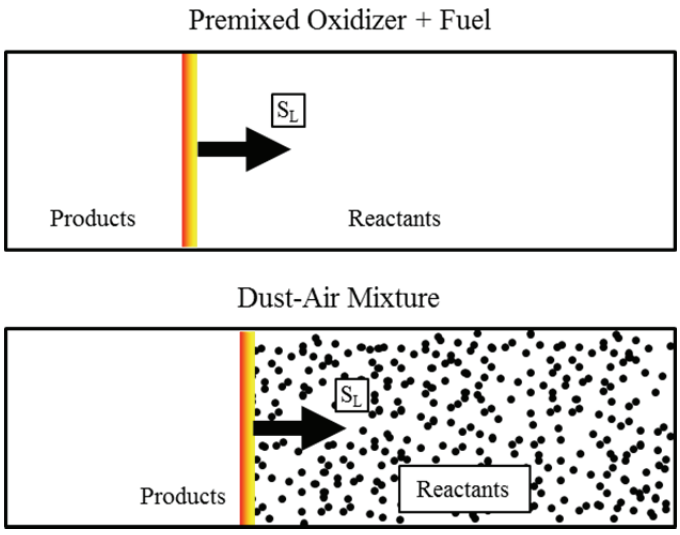

Figure 6 Schematic of a flame propagating through a combustible medium at the laminar flame speed S_L.

Research in Dust Explosions

Various methods have been used to better understand the flammability characteristics of a dust explosion. These methods include a Bunsen burner technique, a long vertical duct, and the closed bomb

method. Each technique presents its own advantages and limitations as is discussed in the following sections.

Bunsen Burner

The Bunsen burner technique has been used extensively with homogeneous mixtures in the vapor phase, due to its simplicity (Badin et al., 1949; Clingman et al., 1953; Gibbs and Calcote, 1959). This system typically involves a calibrated gas handling system to adjust the equivalence ratio and speed of the flow. The premixed fuel and oxidizer travel up a cylindrical tube, and a stationary, conical flame forms at the exit of the tube. To calculate the burning velocity with this method, the volumetric flowrate is measured and divided by the area of the tapered reaction zone.

For research in heterogeneous dust-air mixtures, the Bunsen burner approach is less common, due to technical challenges associated with creating the reactant blend. Goroshin et al. (1996) introduced aluminum dust particles upstream of burner exit plane by using a syringe injection technique. In this work, the burning velocity was determined by dividing the total mass flow rate by the area of the measured flame surface. Dahoe et al. (2002) also implemented a powder burner to stabilize laminar cornstarch-air dust flames to measure the laminar burning velocity. The dust dispersion system consisted of a glass tube in which combustible particles are fluidized together with a number of glass beads. The dust-laden flow is regulated by means of a porous plate. Laser Doppler anemometry was utilized for measuring the burning velocity at various locations inside the reaction zone.

Vertical Duct

In this method, a combustible dust is dispersed in a long vertical duct of varying cross-sectional geometry and is ignited from one end, typically the bottom. A flame travels upward and its spatial velocity is the most common form of characterization. This type of measurement technique has been used by several researchers throughout the literature using organic dusts (Krause and Kasch, 2000; Proust, 2006a; Proust, 2006b; Proust and Veyssiere, 1988; Veyssiere, 1992; Wang et al., 2006) and aluminum (Escot Bocanegra et al., 2010).

Krause and Kasch (2000) investigated the role of turbulence on the flame propagation through organic dusts, such as cornstarch, lycopodium, and wheat flour. Their apparatus was a vertically oriented circular tube, 2 m in length and a 100-mm diameter, and was open at the top. Dust samples were placed at the bottom of the tube and dispersed with a prescribed airflow. Proust (2006a, 2006b) measured laminar burning velocities of cornstarch, lycopodium, and sulphur flour using a 10-cm square cross-section duct with a height of 1.5 m. The facility is equipped with a dust-air suspension generator at the bottom with a gate valve at the top. The heterogeneous mixture is allowed to fill the entire chamber, at which point it is considered completely quiescent. When the desired conditions are achieved within the test section, the mixture is ignited from the bottom and the flame propagates upward. With this apparatus, the square cross-section of the apparatus provides the ability to directly measure the flame transmission. Upon inspection of experimental images, the flame is not perfectly planar and exhibits a parabolic shape due to interaction with the duct walls, which adds to the complexity of the analysis and raises concern about the validity of the results. Proust and Veyssiere (1988) and Veyssiere (1992) used the same dispersion and measurement technique, but with a different apparatus that was 3-m long and had a 20-cm square cross-section. Wang et al. (2006) had a similar apparatus (780-mm height and 160 mm × 160 mm cross-section) and similar dispersion system to measure upward flame velocity using a high-speed camera. The work also sought to characterize dispersion-induced turbulence by implementing a PIV system.

Escot Bocanegra et al. (2010) experimented with flame propagation in aluminum powders consisting of two different particle sizes in the micro- and nanometer range (4.8 μm and 187 nm). The vertical tube had a relatively small length of 180 mm compared to other facilities with an internal diameter of 14 mm. Aluminum particles were placed at the bottom of the tube on a metal filter and were dispersed into the chamber by actuating a valve that released a blast of compressed air. However, for this experimental setup, the dust-air mixture was ignited at the top of the duct, instead of the bottom like the majority of the preceding experiments in the literature, and the downward flame propagation was measured by numerically analyzing images recorded with a high-speed camera. The primary focus of their work was to compare experimental observations of flame velocity and maximum temperature with numerical predictions of a three-stage particle combustion model.

Closed Vessels

The most common experimental facility used with combustible dusts is the closed vessel, or more commonly referred to as the constant-volume bomb. With this approach, a sample of dust is dispersed within the chamber and centrally ignited with a pyrotechnic igniter. A more detailed description of this methodology is provided in the following section. Most constant-volume bombs used in the literature are spherical, although cylindrical geometries are also used but are less common. Regardless of the geometry, there is an inherent risk of uncertainty associated with turbulence generated within the vessel by the chosen method of dispersion. Many researchers have attempted to quantify this artifact, that is particular to each system (Bradley et al. 1988; Dahoe et al., 2001; Pu et al., 1990; Zhen and Leuckel, 1997), and others do not address the presence of turbulence.

Much additional work has been conducted in an effort to better understand the explosive characteristics of organic dusts. Amyotte and Pegg (1989) investigated the range of explosive concentrations for lycopodium using the 1.2-L, cylindrical Hartmann Bomb. This study also attempted to characterize the induced turbulence within the vessel using a plexiglass replica of the rig in association with laser Doppler anemometry (LDA) measurements. Bradley et al. (1988) measured turbulent burning velocities of premixed cornflour-air using high-speed laser schlieren cine photography and using LDA in a fan-stirred explosion bomb. The facility was cylindrical in geometry with a length and diameter of 304 mm. Images were taken from a viewing aperture with a diameter of 150 mm. Cashdollar and Chatrathi (1992) quantified the minimum explosive concentrations of gilsonite dust and bituminous coal dust using the Bureau of Mines 20-L chamber and the Fike 1-m^3 chamber. Continillo et al. (1991) utilized the Siwek 20-L spherical bomb to investigate several coal dusts by varying oxygen concentrations and initial pressures. Dahoe et al. (1995) constructed a strengthened, 20-L spherical bomb to perform experiments with combustible dusts at elevated pressures. After its construction, there was an effort to quantify the induced turbulence within the vessel from the dispersion of cornstarch (Dahoe et al., 2001) and predict the pressure rise within the vessel using a three-zone model that takes into account the flame thickness (Dahoe

et al., 1996). Pu et al. (2007) determined a burning velocity which was derived from pressure-time histories obtained with corn starch and coal dust in the 20-L sphere and two cylindrical vessels of 7 and 22 L.

In addition to organic dusts, characterization of the explosive tendencies of metallic dusts is also of interest. Hertzberg et al. (1992) and Cashdollar and Zlochower (2007) investigated a large array of metallic and other elemental dusts using the Bureau of Mines 20-L sphere by reporting explosion limits as well as dynamic pressure rises and temperatures within the vessel. Soundararajan et al. (1996) gathered samples of iron sulphide dusts from a working mine in Canada and tested its explosive characteristics over a range of particle sizes in the Siwek 20-L spherical bomb.

Aluminum dust has been extensively studied using the constant-volume bombs and continues to be of interest due to its energetic combustion properties. Lin et al. (2010) studied nano-aluminum particles with three distinct diameters of 35-, 75-, and 100-nm and reported rates of pressure rise with varying concentrations of each particle size. Dufaud et al. (2010) studied aluminum dusts in the 20-L sphere by varying dust concentrations, particle size, and humidity levels and measuring pressure traces for each condition. Huang et al. (2009) calculated the laminar flame speed from kinetic theory and found only a slight increase as the equivalence ratio went from lean conditions to stoichiometric. The predicted values in this work were compared to data obtained from closed vessels.

The following section provides experimental details on the constant-volume bomb approach and the traditional data recorded with this methodology. A closer look at the experimental difficulties noted throughout the literature associated with the dust injection process for this approach is presented, and areas where improvements can be made to obtain ideal conditions for direct measurement of flame propagation in dust-air mixtures are identified.

Constant Volume Bombs

The typical procedure followed for dust explosion experiments in closed-vessel facilities is shown in Figure 7, where the process is divided into three stages. First, the rigid vessel is filled with approximately 1-atm air, depending on the desired conditions. Particles of interest are loaded into a

container at the bottom of the rigid vessel. The particle container is commonly a smaller pressure vessel and is pressurized to a level that will transfer all the dust into the main experimental apparatus when a valve is actuated. Specific designs and geometries of the dust container and dispersion nozzle system vary throughout the literature, but the concept remains the same. The pressure within the experimental chamber is evacuated to a level such that the equilibrium pressure is 1 atm between the two vessels. Second, particles are dispersed into the test chamber using a controlled, strong blast of compressed air, which consequently produces turbulence within the facility. There is also an inherent concern about the dust uniformity and test-to-test repeatability of the particle distribution as a result of the dispersion process. The third step occurs several milliseconds after the particles have been dispersed. At this point, the dust-air mixture is ignited at the vessel center, and the resulting flame will propagate outward. Again, the delay time between dispersion and ignition varies throughout the literature but is generally less than one second. The pressure rise produced from the combusting dust within the vessel is typically the primary, if not the only, data recorded during the experiment. There is also additional uncertainty about the pressure rise, associated with the use of strong pyrotechnic igniters.

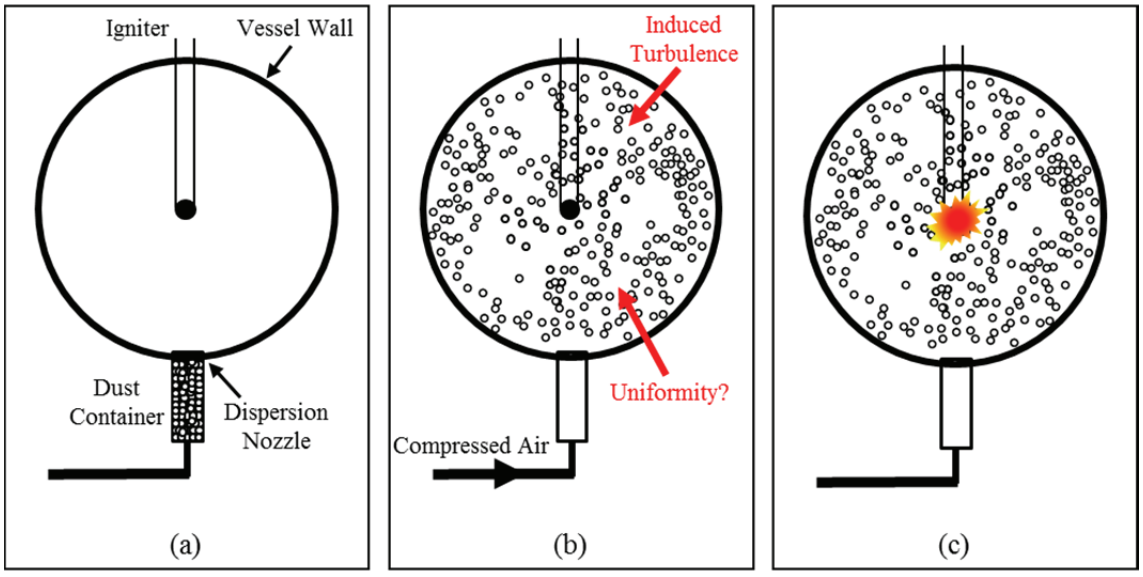

Figure 7 Typical experimental procedure for constant-volume bombs: (a) Dust particles loaded into container located at the bottom of vessel, (b) Particles are dispersed after subjected to a strong blast of compressed air, (c) Ignition occurs at the center of the vessel shortly after dispersion.

Several researchers have calculated a theoretical flame speed using dynamic pressure data (Bradley and Mitcheson, 1976; Luijten, et al., 2009; Santhanam et al., 2010). This use of pressure data is due to the lack of optical access associated with the constant-volume bomb technique. The traditional approach of determining the severity of a dust explosion and probability of occurrence are outlined by several ASTM and ISO standards for testing in closed bombs (ASTM 1226, 2010; ASTM 1515, 2007a; ASTM 2019, 2007b; ISO 6184, 1985) as shown in Table 1. A more-detailed description of each dust property can be found in Dastidar et al. (2005).

Table 1 Measured properties of combustible dusts (U.S. CSB, 2006).

Property	Definition	ASTM Test Method	Application
K_{st}	Dust deflagration index	ASTM E 1226	Measures the relative explosion severity compared to other dusts.
P_{max}	Maximum explosion overpressure generated in the test chamber.	ASTM E 1226	Used to design enclosures and predict severity of the consequence.
$(dP/dt)_{max}$	Maximum rate of pressure rise	ASTM E 1226	Predicts the violence of an explosion. Used to calculate K_{st}.
MIE	Minimum Ignition Energy	ASTM E 2019	Predicts the ease and likelihood of ignition of a dispersed dust cloud.
MEC	Minimum Explosible Concentration	ASTM E 1515	Measures the minimum amount of dust, dispersed in air, required to spread an explosion. Analogous to the lower flammability limit for gas/air mixtures.
LOC	Limiting oxygen concentration	ASTM standard under development	Determines the least amount of oxygen required for explosion propagation through the dust cloud
ECT	Electrostatic Charging Tendency	No ASTM standard	Predicts the likelihood of the material to develop and discharge sufficient static electricity to ignite a dispersed dust cloud.

A typical pressure trace for a constant-volume vessel is shown in Figure 8. After ignition, the pressure rises quickly within the vessel due to the rapid release of energy from the burning dust. During this rise, the maximum rate of pressure change ($(dP/dt)_{max}$) and the peak pressure (P_{max}) are measured. After this maximum pressure is reached, the pressure within the vessel steadily drops due to heat exchange between the hot combustion products and the vessel wall. These parameters are recorded over a wide range of dust concentrations and plotted as a function of concentration, illustrated in Figure 9. Note the scatter in the data plotted in the figure. This scatter is likely due to uncertainty associated with the level of turbulence within the vessel, which can vary from experiment-to-experiment. From this trend, a critical dust concentration is obtained where both the $(dP/dt)_{max}$ and P_{max} occur.

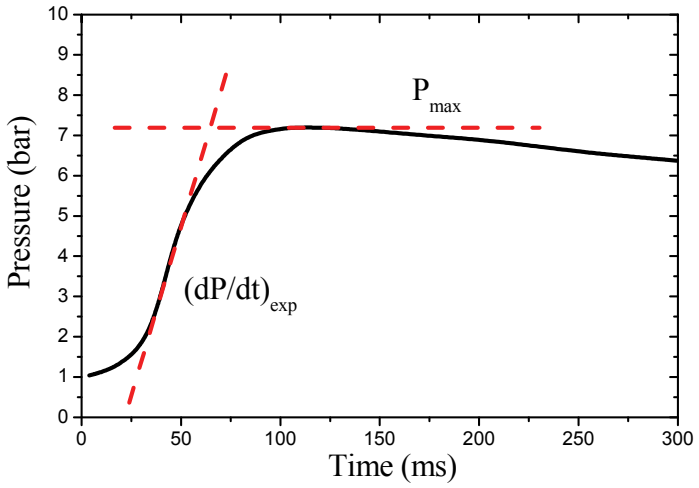

Figure 8 Example pressure curve as a function of time for a typical dust-air experiment in a closed-vessel. Data borrowed from Dahoe et al. (2001).

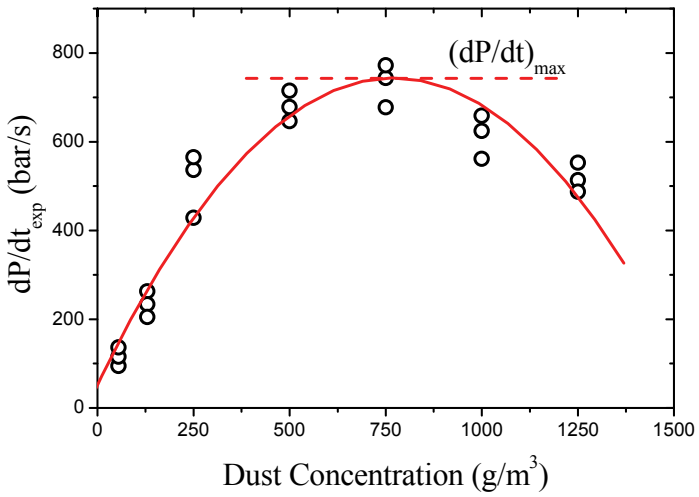

Figure 9 Example of maximum *dP/dt* measured over a range of dust concentrations using the 20L vessel. Data borrowed from ASTM E1226 (2010).

It can be seen from the process outlined in Figure 7 that the burning rates derived from pressure traces are vessel dependent. A larger vessel will have different characteristics associated with the transient flow compared to a smaller vessel. This size dependence can in turn affect the level of dispersion and ultimately the measured parameters. The data can be greatly influenced by the ignition delay time (defined as the time period between instant of injection/dispersion and the ignition event) and the vessel volume. The burning velocity is a fundamental parameter of the combustion process and depends less on the facility and more on the reactive properties of the fuel and oxidizer. However, direct measurement of flame propagation in these heterogeneous mixtures using the constant-volume bomb technique is uncommon in the literature.

CHAPTER III

EXPERIMENTAL FACILITY AND APPROACH

Project Goals

Due to the large amount of uncertainty associated with traditional test methods involving constant-volume bombs, a different approach was taken herein in an effort to achieve ideal experimental conditions for direct measurement of flame propagation in heterogeneous mixtures. The experimental capability of the existing laminar flame speed facility at Texas A&M University (described in the following section) can be adapted to accommodate heterogeneous mixtures of dust and air. A unique aspect of this equipment is the ability to produce high-speed images of the flame growth as a function of time. This capability presents the opportunity to produce quantitative data from direct observation of heterogeneous flame propagation.

In addition to the experimental flame speed images, the conventional dynamic pressure data can be obtained for the combustible dusts investigated. These data can also be used for determining traditional parameters such as P_{max}, $(dP/dt)_{max}$, and K_{st}. By determining these parameters, direct comparison can be made with other values published throughout the literature.

Flame Speed Facility and Visualization Technique

The flame speed facility utilized in this work consists of a constant-volume, cylindrical vessel with optical access located on each end, a Z-type schlieren imaging technique with a high-speed camera, a laser diagnostics station, a gas-handling manifold for filling and vacuuming purposes, and a spark ignition system. The initial pressure of a fuel-oxidizer mixture in the vapor phase can increase by a factor of 10 when ignited. Although the cylindrical bomb is designed to withstand the pressures, an extra measure of safety is implemented into the facility. All experimental equipment is housed within a steel-reinforced, concrete filled blast wall and blast door configuration for an extra level of safety, depicted in Figure 10. During a particular experiment, the blast door remains closed, and access to the apparatus is limited. All

aspects of the experimental procedure are handled remotely outside of the blast wall from the gas-filling manifold. This configuration allows for mixtures to be created within the vessel without personnel entering the room. As an additional level of safety, all experiments are conducted from the control station, which is located in a completely separate room of the facility. From this location, the spark ignition system and high-speed camera are controlled.

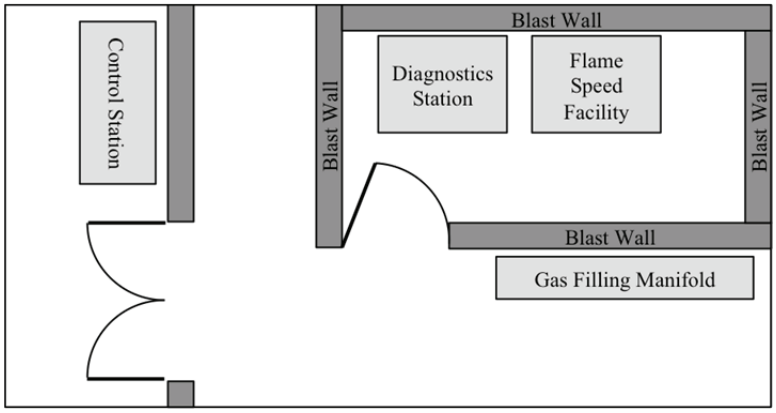

Figure 10 Floor plan layout of laboratory at Texas A&M University.

The cylindrical bomb facility shown in Figure 11 is fabricated out of aircraft-grade 7075-T6 aluminum alloy and is designed to accommodate experiments with initial pressures up to 15 atm at room temperature. It has an internal diameter of 12.0 inches (30.48 cm), an internal length of 14.0 inches (35.56 cm), and a wall thickness of 1.5 inches (3.81 cm). Optical access is provided at each end of the cylinder with fused quartz windows. Each window is 8 inches (20.32 cm) in diameter and 2.5 inches (6.35 cm) thick. The viewing aperture associated with each optical access point has a diameter of 5 inches. Ignition electrodes made from Alloy X rods with a diameter of 0.035 in are located at the top and bottom of the cylinder that point towards each other, meeting at the center of the vessel but separated by a small gap where a spark initiates combustion. Power to the ignition system is controlled with a GwInstek GPR-1810HD constant-current power supply, a 10-μF capacitor, an automotive coil, and a solenoid switch. After igniting the fuel/oxidizer mixture, a flame propagates spherically outward from the center. Dynamic pressure data of the combustion event are recorded via an Endevco 8511A piezo-resistive pressure

transducer. The signal from the transducer sent to a computer-based oscilloscope board from Gage Applied Sciences (5 MHz, 16 bit resolution) and is interpreted using GageScope data acquisition software.

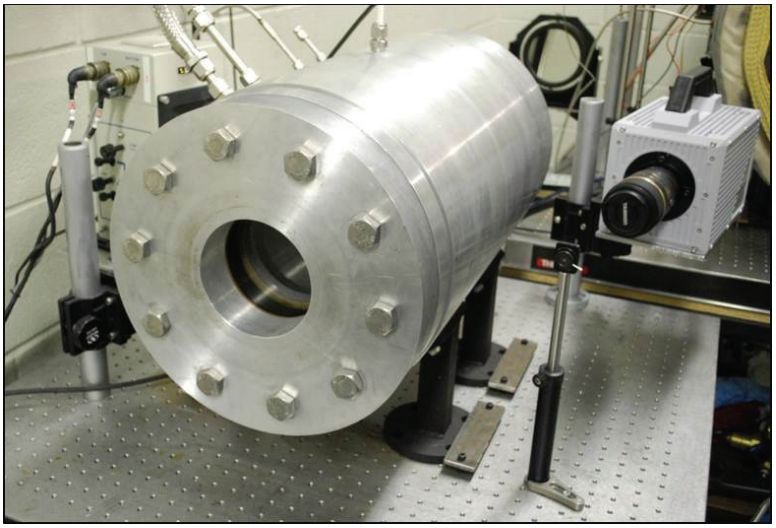

Figure 11 Experimental laminar flame speed facility.

Flame propagation is recorded for each experiment using a Z-type schlieren setup in the fashion suggested by Settles (2006). A schematic of the setup associated with the cylindrical bomb facility is shown in Figure 12. Light from a mercury arc lamp is collimated using an f/8 parabolic mirror with a 6-inch diameter and directed through the optical windows of the experimental vessel. A second parabolic mirror located on the other side of the vessel focuses the collimated beam into a high-speed camera.

The camera used in this study is a Photron FastCam SA1.1. Before the light enters the camera, a circular pinhole aperture is placed at the focal point to cut off a percentage of the beam. This circular aperture emphasizes the density gradients across the reaction zone yielding a clearly defined spherical flame surface. Flame growth is recorded from ignition to when the flame ball becomes larger than the viewing aperture. Images obtained from the high-speed camera are post-processed using a Matlab script that tracks the flame growth as a function of time. Flame radii are calculated by fitting a circle to the outer edge of the flame based on six radial tracking points as described by Lowry et al. (2011). The laminar flame speed is then calculated using relationships described in more detail by Lowry et al. (2011) and also

by de Vries (2009). Results from the post-processing script were analyzed based on the linear relationship given by Eqs. (1)-(3) (Brown et al., 1996; Dowdy et al., 1990; Markstein, 1964).

$$S_{L,b} = S_{L,b}^{o} - L_{m,b}\alpha \tag{1}$$

Where $S_{L,b}$ is the burned, stretched laminar flame speed (and is equivalent to *dR/dt*), $S_{L,b}^{o}$ is the burned, un-stretched laminar flame speed, $L_{m,b}$ is the burned Markstein Length, and α is the flame stretch defined by Eq. (2). In this equation, A represents the surface area of the flame ball, and R is the corresponding flame radius.

$$\alpha = \frac{1}{A}\frac{dA}{dt} = \frac{2}{R}\frac{dR}{dt} \tag{2}$$

The relationship for α in terms of radius was substituted into Eq. (1) and integrated to obtain the instantaneous flame radius. This result is presented in Eq. (3).

$$R = S_{L,b}^{o}t - 2L_{m,b}\ln(R) + C \tag{3}$$

Where t is time, and C is a constant of integration. The burned, un-stretched laminar flame speed and burned Markstein Length are calculated from a linear regression using experimental data for the flame radius as a function of time in Eq. (3). For the analysis presented herein, only values for the burned, un-stretched laminar flame speed are presented. Eqs. (1)-(3) are derived for gas-phase systems, but are applied to the heterogeneous systems investigated herein as an initial attempt to quantify such systems.

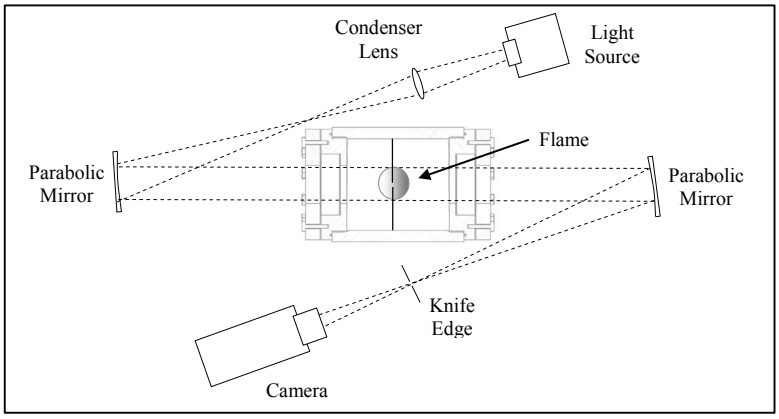

Figure 12 Schematic of experimental flame speed facility and flame imaging technique at Texas A&M University. Image from de Vries (2009).

Powder Injection Approach

Two methods of powder injection are investigated herein. The first is the "direct-injection" approach that is illustrated in Figure 13. In this method, particles are loaded into a 1/2-inch stainless steel tube at the bottom of the vessel. The tubing is bent in a U-shape to hold the particles. The tubing is connected to the gas-handling manifold where dispersion is controlled by a pneumatic valve and a pressurized blast of air. The exit plane of the tubing is just below the line-of-sight of the Z-type schlieren optical pathway. The second technique investigated herein is the "side-vessel" methodology (described with greater detail in to following paragraph) where the heterogeneous mixture is created in a secondary vessel and then transferred to the main experimental flame speed facility. The theory behind the side-vessel methodology is that larger particles and agglomerates will separate from the main mixture before it is transferred to the aluminum flame speed vessel, providing a more uniform particle size distribution when the experiment is conducted. This thesis considers both procedures although the secondary "side vessel" methodology is preferred.

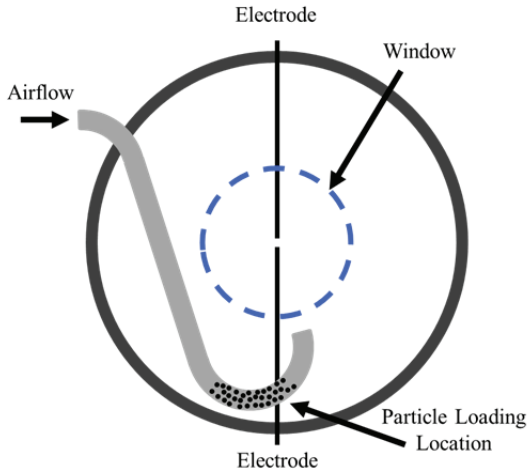

Figure 13 Schematic of "direct-injection" technique depicted in a radial cross-section of aluminum flame speed bomb.

Illustrated in Figure 14 is the powder injection approach employed herein. This technique utilizes an auxiliary vessel where mixtures are made and then transferred into the main experimental facility. This method is summarized in four steps. In the first step (Figure 14a), dust particles are loaded in the Aerosol Injector, which is mounted directly to the secondary Aerosol Mixing Vessel (AMV). The AMV is connected to the Aluminum Flame Speed Vessel with a 1/2-inch flexible Teflon transfer tube. Both vessels are isolated by means of a manually controlled shut-off valve. In the second step (Figure 14b), the particles of choice are dispersed into the secondary vessel by actuating the injection device. This method of creating the dust-air mixture in a secondary vessel by employing an aerosol injector has been proven to promote uniform particle distribution (Kalitan and Petersen, 2007; Kalitan et al., 2006).

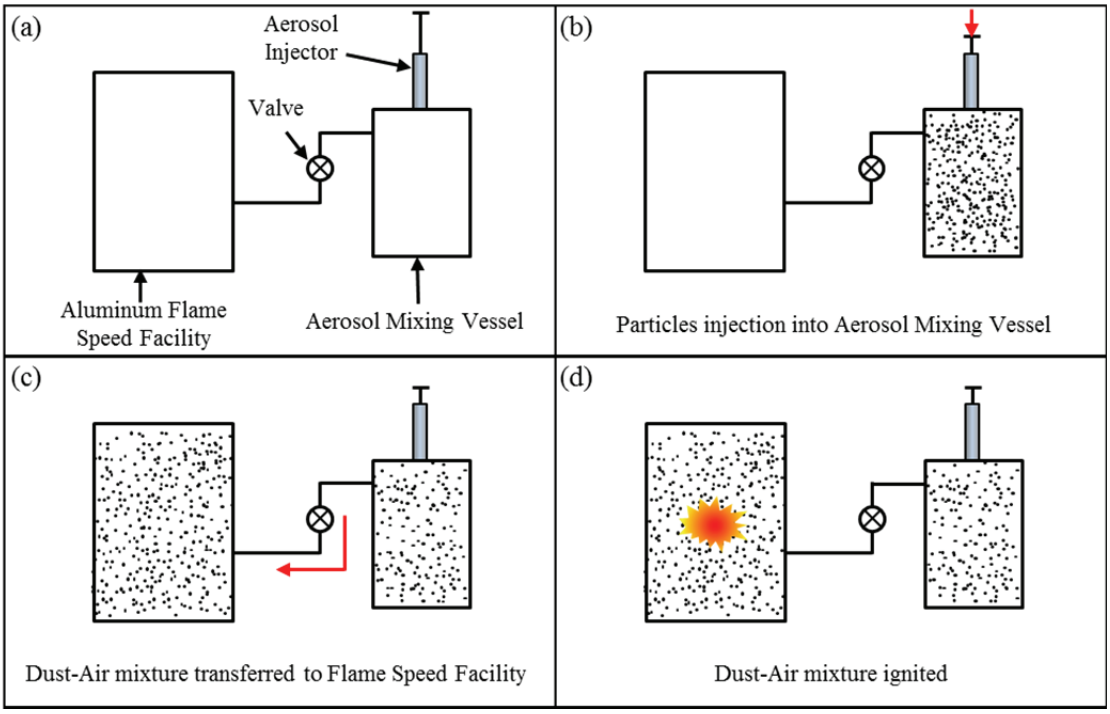

Figure 14 Experimental approach adapting previously developed particle injection technique by Kalitan and Petersen (2007). (a) Particles are loaded into the aerosol injector that is mounted directly to the Aerosol Mixing Vessel (AMV), (b) Particles are dispersed into the AMV, (c) The heterogeneous dust-air mixture is transferred to the Experimental Flame Speed Facility, and (d) Dust-air mixture is ignited at the center of the vessel with an electronic spark and subsequent flame propagation is recorded using the imaging technique.

Particle distribution and turbulence intensity can be qualitatively assessed within the AMV by means of a laser extinction technique. Details of this measurement technique are provided in the following section. Upon verification of the overall particle distribution within the AMV, the heterogeneous mixture is then transferred to the experimental vessel by opening a valve (Figure 14c). After the mixture is transferred into the aluminum experimental vessel, it is allowed to reach a quiescent state prior to ignition (Figure 14d). Typical wait times are on the order of 1-2 minutes or less depending on the mass loading and size of the particles. Longer and shorter wait times are generally expected for higher and lower particle concentrations, respectively. Larger particles will settle to the bottom of the vessel quickly, and the smaller particles stay suspended for extended periods of time. To illustrate this concept, consider the terminal settling velocities for particles of different diameters, presented in Table 2. Terminal settling velocities were calculated by assuming spheres of constant density, traveling at a constant velocity with only gravitational and drag forces acting on the body. A 10-micron particle will travel a distance of 10 mm in less than 4 seconds, whereas a 100-nanometer particle will take over 3 hours to travel the same distance.

Table 2 Terminal settling velocities of standard density, spherical particles at 293 K and 1 atm. Data taken from Hinds (1999).

Particle Diameter (µm)	Terminal Settling Velocity (µm/s)
0.001	6.9×10^{-3}
0.01	0.07
0.1	0.88
1	35.0
10	3.1×10^{3}
100	250×10^{3}

The existing high-speed imaging capability is used to directly track the growth of the flame kernel in the heterogeneous mixture. These images are used to compute the laminar burning velocity, as previously described. Dynamic pressure data of the combustion event are also acquired for each

experiment. These data provide a convenient way of obtaining traditional dust explosion parameters of P_{max}, $(dP/dt)_{max}$ and K_{st}, which can then be directly compared to the published values in the literature.

Component Design

Aerosol Injector

Kalitan and Petersen (2007) designed the particle injection system used herein for the secondary vessel approach. The aerosol injector was modeled after a similar device described by Parker et al. (2001) that was used in shock-tube studies and was mounted directly to the experimental facility. A schematic of the proposed particle injector is shown in Figure 15. The assembly consists of three main components: the piston cylinder, flow-splitting plate, and nozzle section. A commercially available Humphrey 6-D-6 stainless steel air cylinder with the end removed was used for the piston-cylinder device. The flow-splitting plate was fabricated using a rapid prototyping technique with a nylon-based polymer resin. The nozzle section was machined from 304L stainless steel. Seals between each component were made with Buna-N o-rings. Details on the design of the Nozzle Section and Flow Splitting Plate are shown in Figure 16. Only basic dimensions are provided in this figure for clarity. Detailed drawings of both components are provided in the Appendix.

Particles are loaded into the cavity of the nozzle section, and a 120 mesh is placed between the dust sample and the flow splitting plate. The particles are then dispersed into the vessel by a manually driven piston. Airflow created by the piston travels through the orifices in the flow splitting plate, promoting the transfer of dust particles into the AMV.

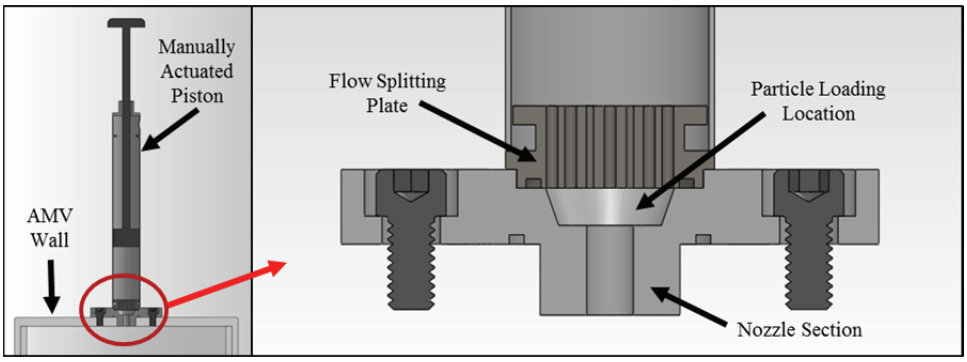

Figure 15 Cross-sectional view of the Aerosol Injector Assembly and its three main components: (1) Manually Actuated Piston, (2) Flow Splitting Plate, and (3) Nozzle Section.

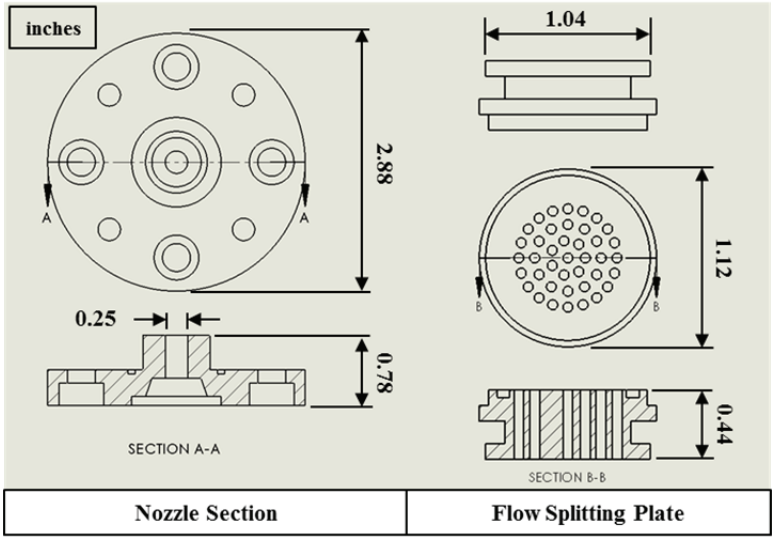

Figure 16 Dimensions for Nozzle Section and Flow Splitting Plate.

Aerosol Mixing Vessel

The AMV is being developed in two phases. The first phase (presented in this thesis) serves as proof of concept and is constructed of commercially available, 8-inch, schedule 40 PVC pipe and fittings as shown in Figure 17. This vessel is designed to have the same internal volume as the aluminum flame speed facility. Fluidic connections to the AMV are made with 1/2-inch stainless steel NPT fittings from Swagelok. Vacuum and filling operations are conducted through a single port at the end of the AMV using 1/4-turn shut-off valves. The particle injector assembly is mounted on the flat PVC end cap with 1/4-20

socket head caps screws, perpendicular to the piping connection that is meant to transfer the heterogeneous mixture to the aluminum flame speed vessel. The distance between the transfer tube and fill/vacuum connections was selected for compatibility with the Z-type schlieren optical pathway. A removable endcap provides access to the PVC AMV for general housekeeping between experiments. As a safety precaution, a grounding wire is installed inside the vessel to eliminate the potential build-up of static electric charge from movement of the dust.

During a given experiment, the AMV is pressurized to approximately 21 psia, and the flame speed vessel is evacuated to a vacuum of 400 torr. This pressure differential facilitates the transfer of the dust mixtures to the aluminum vessel, and the final pressure equilibrates to 1 atm. The second phase of AMV development will be fabricated out of stainless steel. This second-generation vessel will reflect any lessons learned from the PVC-AMV, and will be a more-permanent facility.

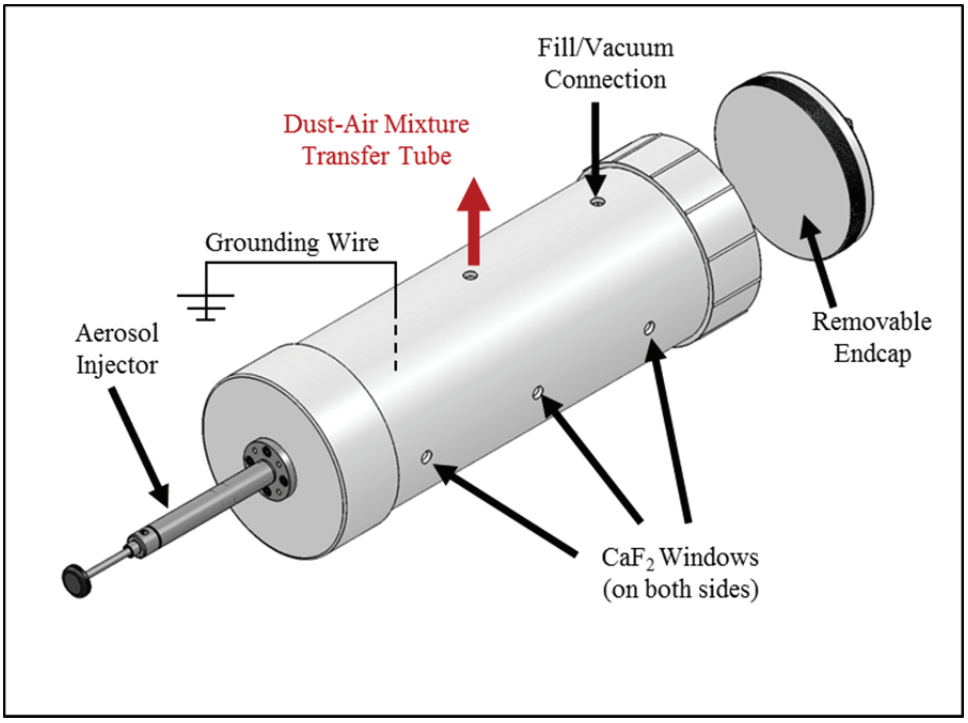

Figure 17 Schematic of Aerosol Mixing Vessel featuring the Aerosol Injector mounted on the flat endcap, plumbing connections, laser diagnostic ports, and a grounding wire to discharge any electrical charge that may be present due to particle collisions.

Laser Diagnostic

Calcium fluoride (CaF_2) window ports can be installed in three locations along the symmetric axis of the AMV, for laser extinction diagnostics. However, the current experimental setup has a single set of CaF_2 windows at the center of the AMV, as shown in Figure 17, to test the effectiveness of the technique before additional ports are added. A 632.8-nm, 5-mW HeNe laser is passed through the AMV, and the intensity is measured before (I_o) and after (I) contacting the heterogeneous mixture. The same process was repeated for the aluminum flame speed vessel, using the fused quartz windows at each end of the cylinder. Two New Focus 2032 photodiodes outfitted with narrowband 632.8-nm filters in association with a series of optics were used to capture the extinction of the laser beam. This configuration is illustrated in the schematic of Figure 18.

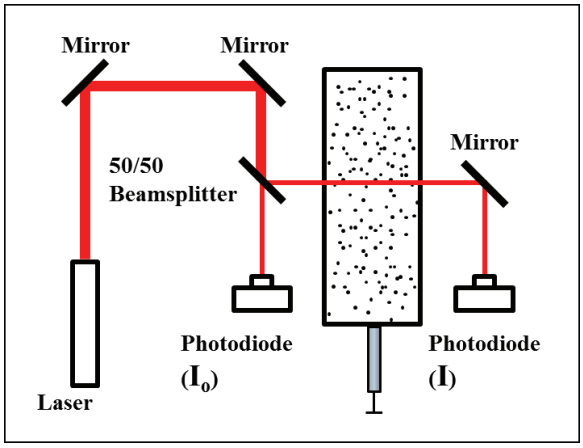

Figure 18 Schematic of laser diagnostic system. Particle uniformity is confirmed from the photodiode signals using the Beer-Lambert law.

The attenuation of light passing through a particulate medium is defined as the optical extinction. As the beam of light contacts the suspended solid particulate, it is scattered and absorbed. The fraction of light scattered and absorbed within the vessel depends on the geometry and material of the aerosol. The laser intensities are then compared using the Beer-Lambert Law shown in Eq. (4) to obtain the extinction (Liebhafsky and Pfeiffer, 1953; Malinin and Yoe, 1961; Pfeiffer and Liebhafsky, 1951; Swinehart, 1962). Where σ_e is the extinction coefficient of the powdered aerosol, and L is the optical path length of the laser

through the aerosol. This equation assumes the presence of a parallel monochromatic light beam passing through an evenly dispersed particulate medium.

$$I/I_o = \exp(-\sigma_e L) \tag{4}$$

The extinction coefficient can be defined as the product of the particle number density, N, and its extinction cross section, C_{ext}, which is represented by Eq. (5). The extinction cross section is defined in Eq. (6) as the sum of the absorption and scattering cross sections.

$$\sigma_{ext} = NC_{ext} \tag{5}$$

$$C_{ext} = C_{sca} + C_{abs} \tag{6}$$

The extinction cross section can be related to the particle geometric cross-sectional area, A_p, by Eq. (7), where Q_{ext} is the extinction efficiency. Higher extinction efficiencies mean that fewer particles are required for a given intensity ratio. A more-detailed derivation can be found in Bohren and Huffman (1998).

$$Q_{ext} = \frac{C_{ext}}{A_p} \tag{7}$$

Solving Eq. (7) for C_{ext}, and substituting the cross-sectional area of a particle in terms of the average particle diameter yields Eq. (8).

$$C_{ext} = Q_{ext} \frac{\pi}{4} d^2 \tag{8}$$

Relating these equations to the optical depth, τ, as described by Signorell and Reid (2011), and the number density of the particulate medium are defined by Eqs. (9) and (10), respectively.

$$\tau = -\ln\left(I/I_o\right) = NC_{ext}L \tag{9}$$

$$N = \frac{\tau}{C_{ext}L} \tag{10}$$

The geometry of nano-particles significantly affects the optical properties. Extensive research has been performed in analyzing the optical properties of Al (and Au) nano-particles. Temple and Bagnall (2011) discuss how the cross-sectional size, shape and aspect ratio affect the extinction peak position and

extinction efficiencies of nano-Al and concluded that their lateral size and shape can be modified to shift their extinction peaks across the visible spectrum. Extinction efficiencies for metallic nano-particles are typically greater than unity. The percentage of scattering and absorption depends on the particle size. The results presented by Chowdhury et al. (2009) show that scattering was dominant in the extinction for nano-Al particles with diameters of 20, 40, 80, and 100 nm.

With this diagnostic, qualitative conclusions can be made on the timing and uniformity of the dispersion method, in addition to providing insight on the level of turbulence in both the AMV and aluminum flame speed apparatus. Implementing these laser diagnostic capabilities provides the ability to characterize the uniformity of the dispersion as well as the particle settling time. The extinction technique can also help identify the critical size of particles that are appropriately suited for this experimental equipment, shown in Figure 19. For example, if a particle is too large, it will settle to the bottom of the AMV before it can be transferred into the aluminum vessel.

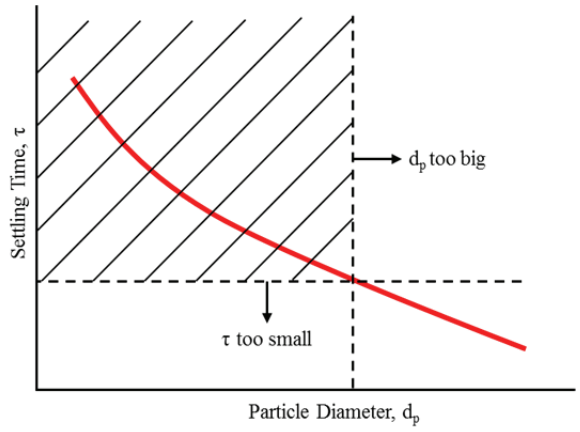

Figure 19 Representative behavior of particle settling time as a function of particle diameter. Shaded area indicates the particle size range that is feasible for this measurement technique. The vertical dashed line shows the critical particle size.

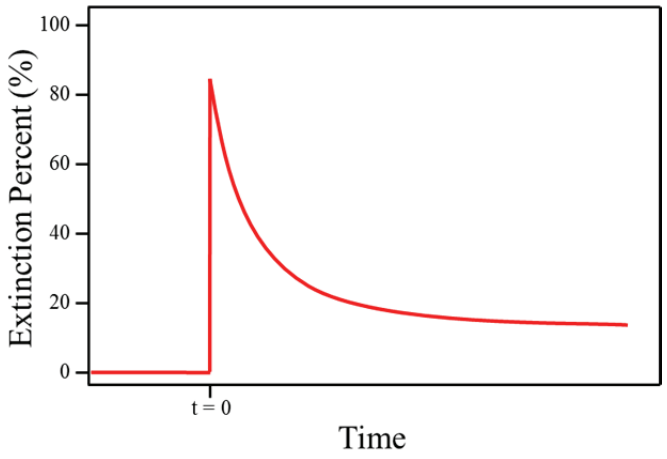

Figure 20 Characteristic extinction "wait-time".

This technique can also provide the necessary information needed to define the overall experimental procedure outlined in Figure 14. Laser extinction measurements can be made on both the PVC-AMV and the Aluminum Flame Speed facilities to define the time period necessary for the turbulence in the heterogeneous mixture to decay and the concentration of suspended particles to each a near-steady state level. A typical extinction measurement is presented conceptually in Figure 20. The extinction exhibits an initial transient behavior due to the momentum imparted from the pulsed dust-laden jets, and then reaches a steady state value as the fluid mechanics within the chamber become quiescent and the larger agglomerates drop out. From this measured time history, two “wait-times” can be defined for each vessel. The wait time for the PVC-AMV, t_1, determines the time period from particle injection to the instant when the transfer valve to the aluminum vessel is opened. The second wait time, t_2, represents the delay prior to ignition inside the aluminum flame speed vessel.

The final assembly of the experimental equipment is shown in the horizontal-view of Figure 21 and the top-view of Figure 22. The PVC-AMV is secured to a dedicated optics table on which the diagnostics are mounted. Part of the schlieren optics are also integrated with this table. Note that flexible Teflon transfer tubing was used to connect the two vessels to minimize any obstruction to the dust-laden flow during the transfer process. In addition, the distance between the PVC-AMV and the aluminum vessel was kept as close as possible.

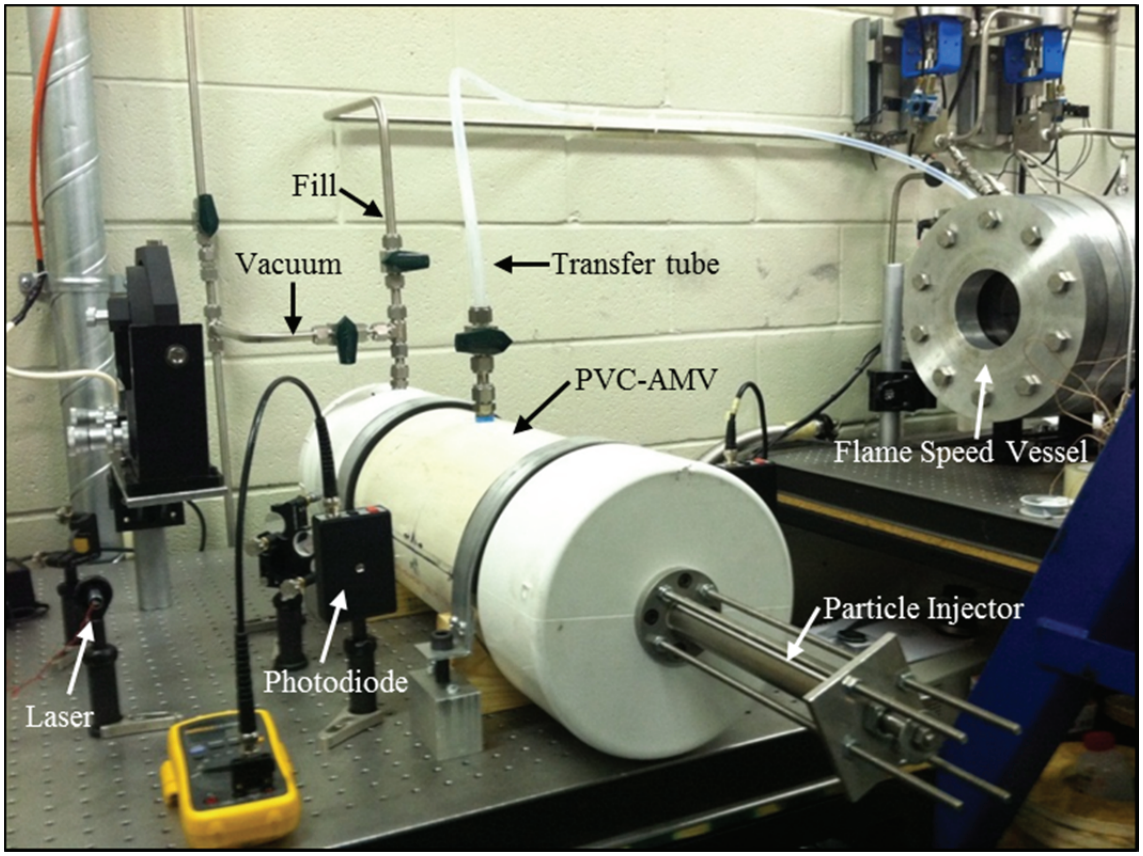

Figure 21 Horizontal view of experimental facility.

Figure 22 Top view of experimental facility.

CHAPTER IV

INITIAL RESULTS

Experiments were performed at atmospheric conditions (~298K and 1atm) using a hybrid mixture of $Al/CH_4/O_2/N_2$. Two different powders were investigated using the laser extinction diagnostic in conjunction with the PVC-AMV. Cornstarch was initially investigated for compatibility with the experimental approach due to its availability and abundance in the process industries. The extinction results indicated that the cornstarch particles were too large for the proposed system and were not investigated further. So, aluminum nano-particles were used and characterized in detail using the extinction diagnostic. The following sections present the experimental parameters, results from the extinction diagnostic performed on both the PVC-AMV and the aluminum flame speed facility, and initial results using a hybrid mixture of $Al/CH_4/O_2/N_2$.

Experimental Parameters

Nano-Aluminum particles used herein were purchased from US Research Nanomaterials, Inc. The average mean diameter of the particles published by the manufacturer is 100 nm. Scanning Electron Microscope (SEM) images were taken of the dust sample and are shown in Figure 23. The image shows a wide distribution of particle sizes with large agglomerates on the order of 100 μm. Several images were taken at a greater magnification, showing the fundamental particle size to be within the sub-micron range, lending validity to the nano-particle size range as quoted by the manufacturer. Aluminum particles are naturally encapsulated with a thin layer of aluminum oxide, Al_2O_3. For the aluminum particles to burn, the naturally occurring outer layer of Al_2O_3 must first be penetrated. This occurs at the melting temperature of approximately 2300 K (Eckhoff, 2003).

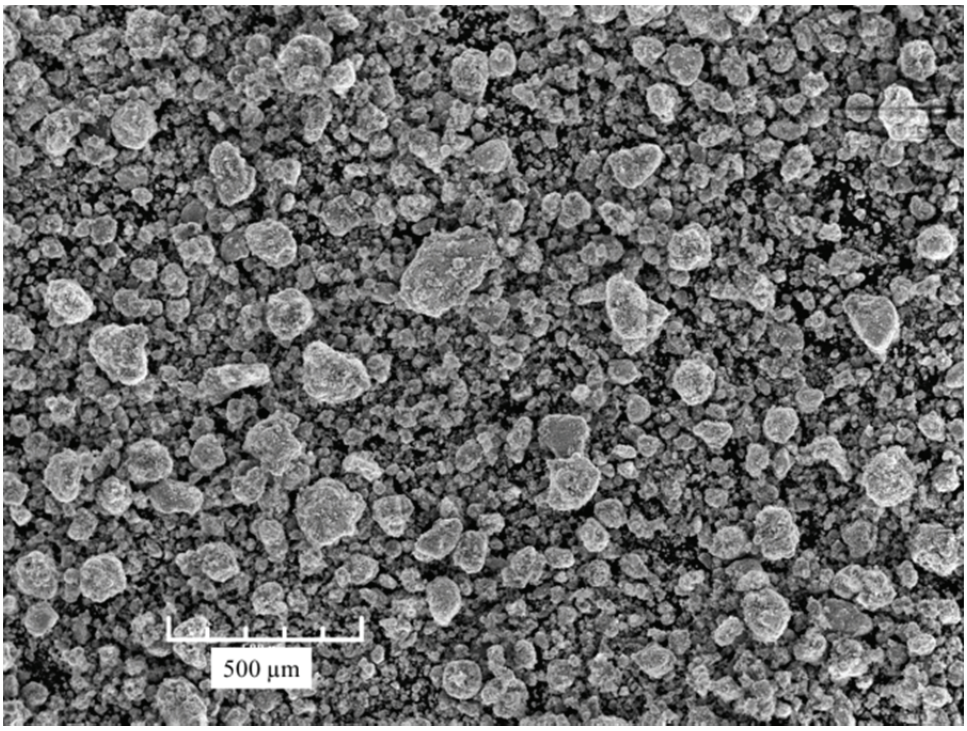

Figure 23 SEM image of nano-Aluminum particles used herein.

As mentioned in Chapter III, the "direct injection" approach using the nano-Al was first taken to validate the ignition and imaging systems with the hybrid mixture of $Al/CH_4/O_2/N_2$. During the initial characterization experiments, it was found that for the typical loadings produced by the first-generation methods herein, a pure powder-air system would not ignite. This inability to ignite was likely a result of the current spark ignition system not capable of producing enough energy to overcome the oxide layer allowing the aluminum to combust. To overcome these challenges presented with the ignition system and to continue with the problem at hand—to demonstrate a system for controlled laminar flame speed measurements in aerosol mixtures—a hybrid blend of nano-aluminum powder with an alkane, oxygen, and nitrogen were considered. The hybrid blend still provides the ability to study the effect of nano-Aluminum particles on the combustion process while ensuring the presence of combustion.

In determining the alkane fuel and oxidizer mixture, one must first consider the adiabatic flame temperature (T_{AF}). Two methods, based on different assumptions, are used to calculate the adiabatic flame temperature from the conservation of energy. The two assumptions made with this equilibrium calculation

are constant volume (V) and internal energy (U), or constant pressure (P) and enthalpy (H). Both of these assumptions and the resulting T_{AF} are plotted in Figure 24 for methane burning in air. At first glance, one might think constant U/V most accurately describes the combustion process in the Aluminum Flame Speed vessel. This assumption gave a T_{AF} that is much higher than the melting point of Al_2O_3 for equivalence rations of 0.7-1.5. However, Lowry et al. (2011) has previously shown that the pressure does not increase over the course of the flame growth from the kernel to the window diameter in the present apparatus, suggesting the more-applicable assumption for this scenario would be the constant H/P. This constraint brought the T_{AF} below 2300 K, implying that the nano-Aluminum particles might not burn at these conditions. Figure 25 shows that changing the type of fuel reacting with air at the same conditions also does not raise the T_{AF} above the 2300 K mark.

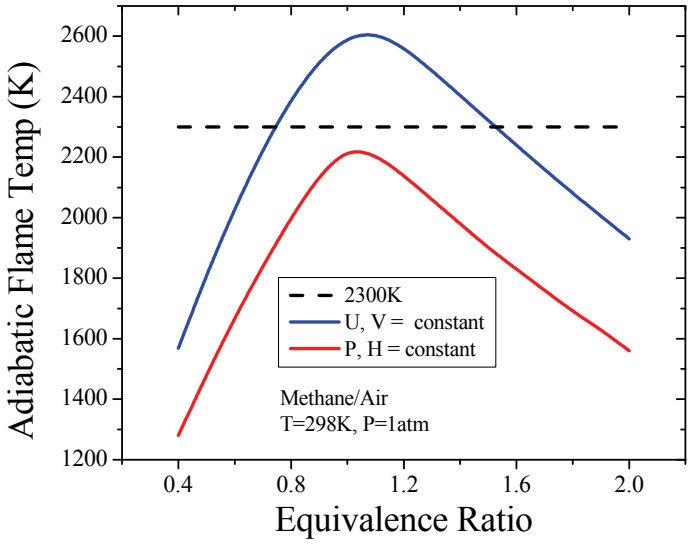

Figure 24 Adiabatic flame temperature as a function of equivalence ratio for methane burning in air with different equilibrium assumptions as predicted using the equilibrium function within CHEMKIN modeling suite.

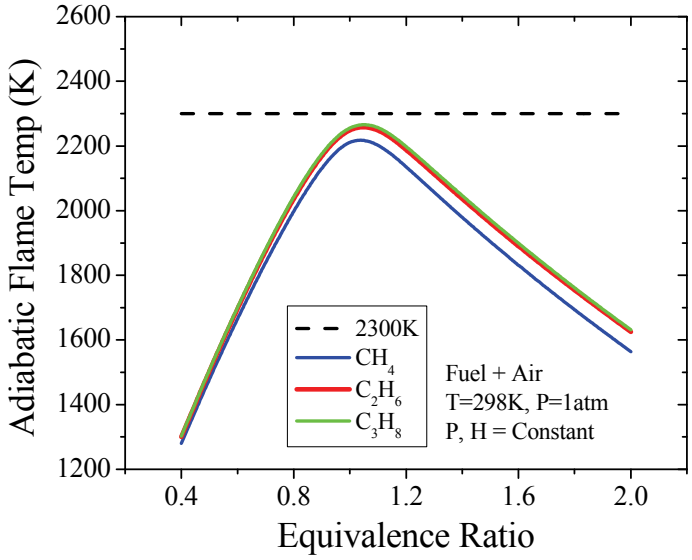

Figure 25 Adiabatic flame temperature as a function of equivalence ratio for C1-C3 alkanes burning with air at atmospheric conditions. Predicted using the equilibrium function within CHEMKIN modeling suite.

To increase the T_{AF} above the melting temperature of the aluminum oxide layer, hence ensuring exposure of the core Al to the reacting gases, the ratio of O_2:N_2 in the oxidizer was varied. This effect on the T_{AF} is shown in Figure 26. By increasing the percent of oxygen in the oxidizer from 21% to 30%, the maximum T_{AF} increased by almost 400 K. As a safety check, the overpressures for these different nitrogen dilution ratios were also estimated and are shown in Figure 27. From this figure, peak pressure increased about 0.75 atm to a maximum value of approximately 9.25 atm with the CH_4/(30% O_2 + 70% N_2) as compared to CH_4/air. These pressure peaks are well within the working limits of the flame speed bomb. Thus, a stoichiometric mixture of CH_4-(30:70 O_2:N_2) was selected as the hybrid mixture and was tested with and without the presence of aluminum particles.

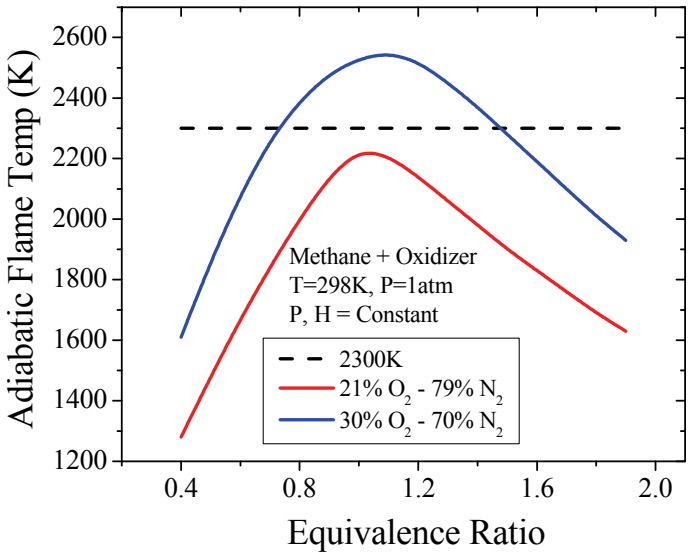

Figure 26 Adiabatic flame temperature as a function of equivalence ratio for methane burning with different ratios of oxygen and nitrogen. Predicted using the equilibrium function within CHEMKIN modeling suite.

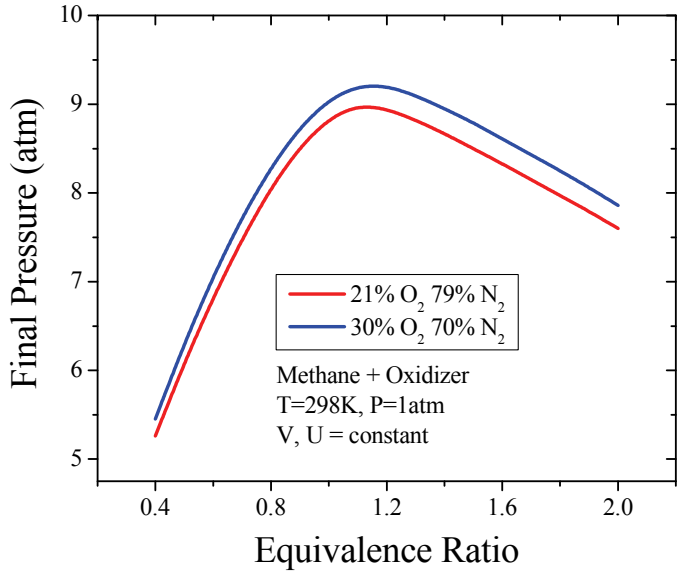

Figure 27 Overpressure vs. Equivalence ratio for methane reacting with different ratios of O_2:N_2 under the constant U/V assumption for a closed system as predicted by CHEMKIN equilibrium solver.

Laser Extinction

To simplify the extinction analysis, particles were assumed to be spherical and have a diameter of 100 nm. This diameter was chosen based off information provided by the manufacturer and the SEM images. To improve the accuracy of the results, an average particle size should be selected using a best fit to the particle distribution function, as explained and performed by Peng et al. (2009). This level of precision is left for future efforts for now. The extinction cross-section defined by Eq. (6) was calculated by assuming a value for extinction efficiency of 0.5 based on values published in the literature for 100-nm spherical aluminum particles at a wavelength of 632.8 nm (Chowdhury et al., 2009; Temple and Bagnall, 2011; Quinten, 2011). The extinction efficiency selected from the literature was used to calculate particle number densities from the measured extinction data.

"Side-Vessel" Method

For each experiment, the PVC-AMV was pressurized to approximately 21 psia, and the aluminum flame speed vessel was evacuated to 400 torr. To characterize the system, nitrogen was used to pressurize the system for safety precautions (rather than with something containing oxygen). For the actual experiment, the hybrid mixture of CH_4-(30% O_2 + 70% N_2) was used as the fluid in both vessels. Particles were injected into the AMV during this pressurized state and transferred to the aluminum flame speed vessel after a period of time. The final pressure between the two vessels was 1 atm. Figure 28 shows the percent extinction recorded in the PVC-AMV during the transfer process for an injector mass loading of 1.03 g. Injection takes place at the first peak of extinction at just over 80%. This large extinction is due to a high concentration of particles traveling with the initial jet from the aerosol injector. The data are presented so that the injection occurs at $t=0$. At approximately 350 seconds, the transfer valve is opened, and a second peak in extinction is measured at about 40%. This second peak is thought to be due to particles being re-suspended due to the sudden mass transfer out of the PVC-AMV. The laser for this particular experiment was located at the center port of the PVC-AMV, directly under the transfer tube. Several repetitions of this scenario were performed, and the results show a strong dependency on the

impulse applied to the aerosol injector piston. Different levels of extinction were recorded (varying as much as 20 percentage points) for the same injector mass load for minute changes in the piston actuation velocity. This finding suggests that a more consistent method of applying the dispersion is necessary for better repeatability.

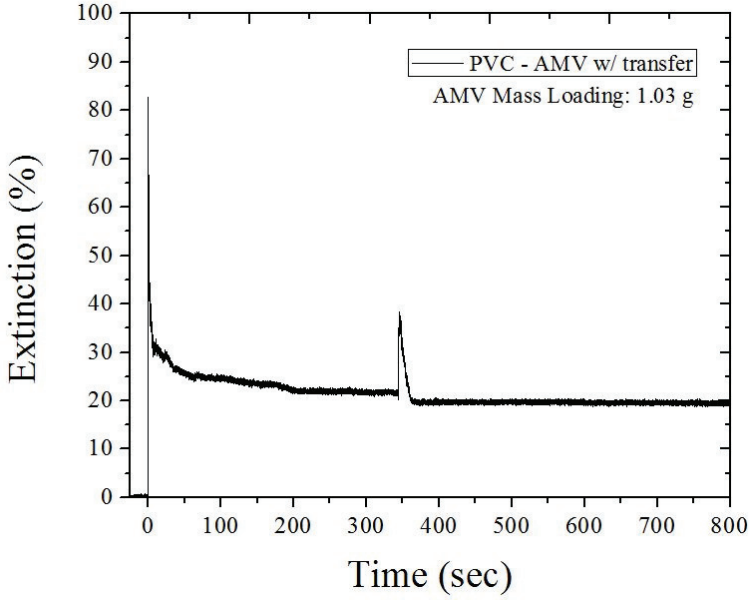

Figure 28 Extinction percent as a function of time for the PVC-AMV vessel and transfer process with an injector mass loading of 1.03 g.

The extinction percentage and particle number densities were measured and calculated, respectively, within the aluminum flame speed bomb using the "side-vessel" methodology. Also for this experiment, 1.03 g of aluminum dust were placed in the aerosol injector before the heterogeneous mixture was made and then transferred. Extinction data are plotted in Figure 29, and the corresponding number density calculation is shown in Figure 30. A peak extinction of just fewer than 10% was measured in the aluminum vessel. The transient behavior in the extinction is present for approximately 50 seconds and then gradually decreases over the 13 minutes it was recorded. In Figure 30, a maximum particle count of 1.2×10^{8} particles/cm^{3} was recorded and dropped below 3.0×10^{7} particles/cm^{3} after about 5 minutes.

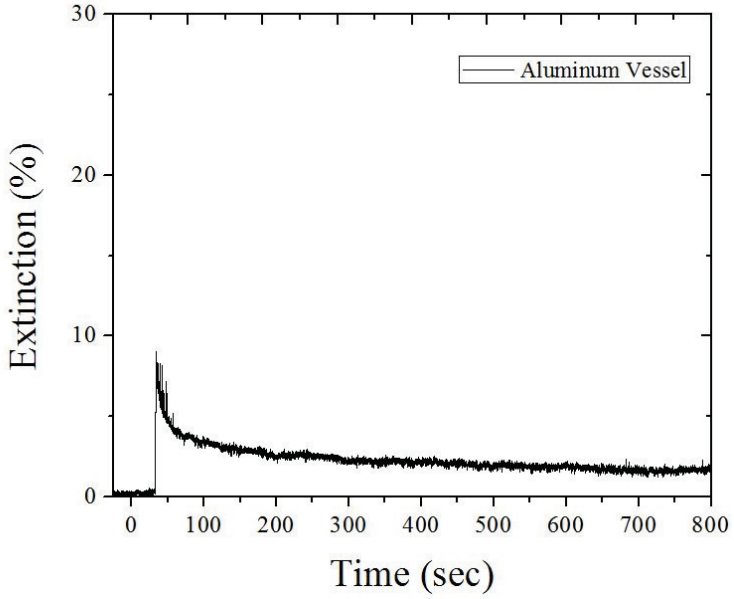

Figure 29 Extinction percent as a function of time for the Aluminum Vessel after the heterogeneous mixture is transferred from the PVC-AMV.

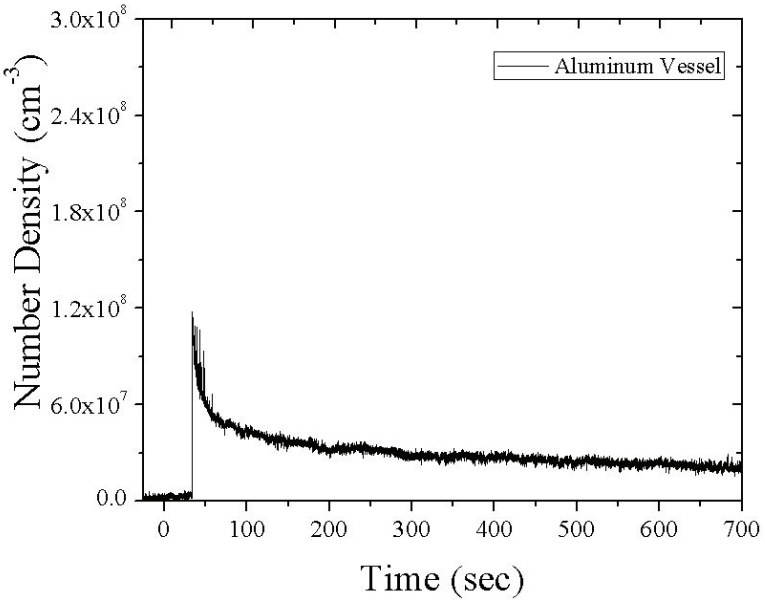

Figure 30 Particle number density as a function of time for the Aluminum Vessel after the heterogeneous mixture is transferred from the PVC-AMV.

“Direct Injection” Method

For the “direct injection” method, particles were placed in a reservoir at the bottom of the cylindrical vessel that was fabricated from 1/2-inch stainless steel tubing, as depicted in Figure 13. The pipe is directly connected to the gas handling manifold where a pneumatically operated valve controls the gas flow entering the vessel. Before dispersion, the vessel is first evacuated and then filled to a pressure of 600 torr using the desired gaseous mixture. After the vessel is filled, the manifold is pressurized to 100 psia using the same gaseous mixture. When the pneumatic valve is actuated, a strong blast disperses the particles, and the final pressure reaches 1 atm. For actual experiments, the hybrid mixture of $CH_4/O_2/N_2$ was used. For characterization purposes, nitrogen was used.

The percent extinction using the aforemention procedure is shown in Figure 31 for two separate instances where 0.25 g of aluminum dust was dispersed within the aluminum flame speed rig. Each trace experiences a 100% maximum extinction and gradually decreases over time. It is interesting to note the envelope of each test is remarkably similar. The two traces are aproximately 5 percentage points different throughout the entire 800 seconds. The particle number density was also calculated for each test using this technique, and the results are plotted in Figure 32. When the particles are dispersed, a maximum number density of about 2.25×10^9 particles/cm^3 was recorded. The number density fell below 5.0×10^8 particles/cm^3 between 50-150 seconds for both tests. Over the period of 800 seconds, the number density remained at about 2.5×10^8 particles/cm^3. More particles were detected from the direct injection approach as compared to the “side-vessel” method from Figure 30 for similar mass loadings. In other words, the direct injection approach seems to break up the potential agglomerates much better than the aerosol injector, so that there are more nano-sized particles that remain suspended at longer times. Results from the “direct injection” approach also suggest a higher degree of repeatability as compared to the aerosol injector technique.

Several simplifying assumptions were made in an effort to estimate the instantaneous mass of suspended aluminum particles within the vessel during the direct injection experiment. As with the extinction efficiency, particles were assumed to be spheres of solid aluminum with diameters of 100 nm. From this, a mass per particle was calculated. Using the particle number density shown in Figure 32 and

the volume of the flame speed bomb, the instantaneous mass of suspended particles within the vessel was estimated and shown in Figure 33. The estimation is based on many simplifying assumptions and is meant to simply validate the number density calculation. As shown in the figure, the suspended mass has a maximum value of 0.08 g and quickly settles to a value of below 0.02 g.

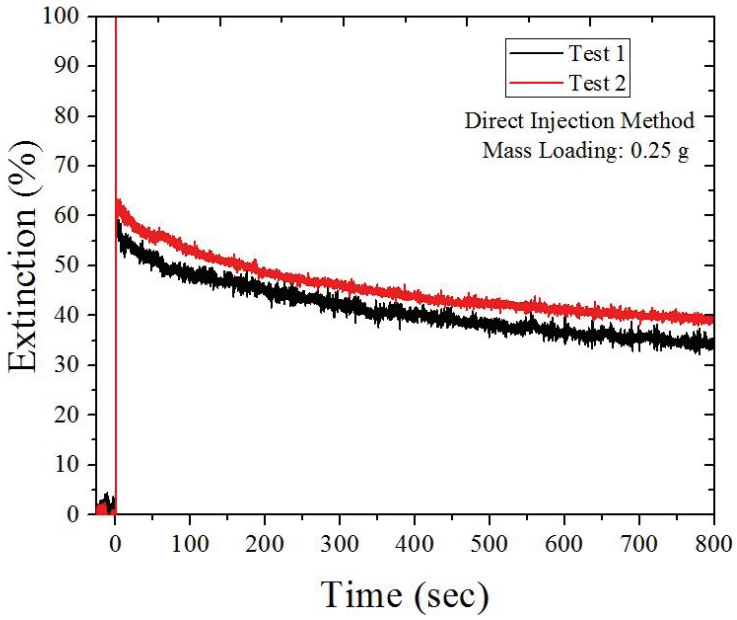

Figure 31 Extinction percent as a function of time for an aluminum mass loading of 0.25 g directly injected into the Aluminum Vessel.

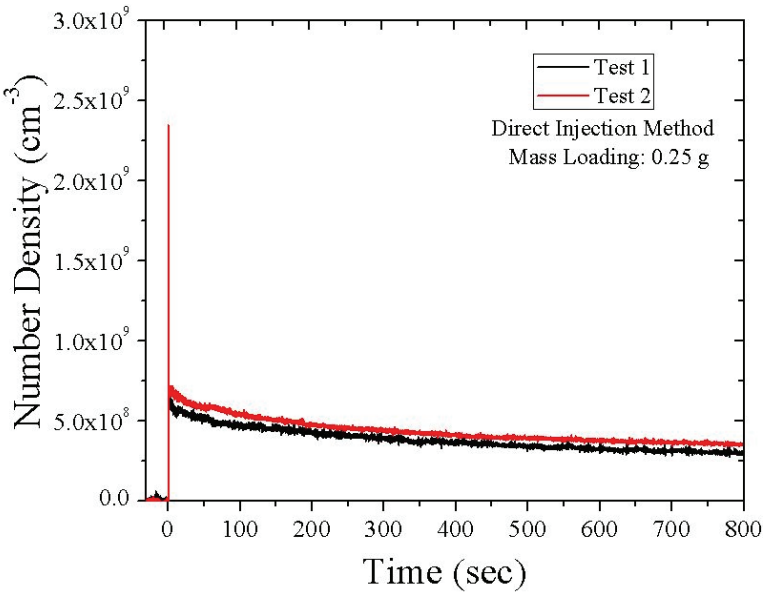

Figure 32 Particle number density as a function of time for an aluminum mass loading of 0.25 g directly injected into the Aluminum Vessel.

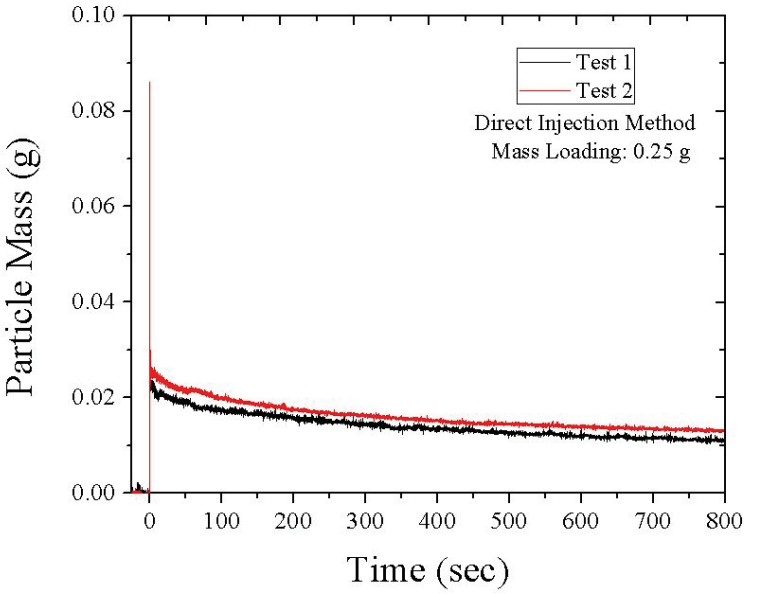

Figure 33 Instantaneous mass of nano-Al particles suspended within the aluminum flame speed vessel as a function of time. Calculated using particle number density and assuming 100-nm, solid aluminum spheres.

Analysis and Flame Images

Initial experiments were performed using the dust transfer method and the procedure outlined in the previous section. Initial results suggested a high dependency on the impulse applied to the piston during the injection process and demonstrated a low level of repeatability. In addition, such few aluminum particles actually transfer into the flame speed vessel compared to the original mass loading applied to the injector. The burning velocity and dynamic pressure response did not reflect a significant presence of aluminum particles when using the aerosol produced in the side chamber.

Aluminum particles were then injected directly into the vessel to initially see if the new ratio of O_2 to N_2 was effective at burning the aluminum nano-particles. This method was also followed to test the sensitivity of the optical and pressure-sensing equipment to the presence of the aluminum. The results from the new hybrid mixtures are compared to previous data for stoichiometric methane-air in Figure 34, and the numerical data for this figure are available in Table 3. The instantaneous mass was interpreted using the data of Figure 33 for each experiment.

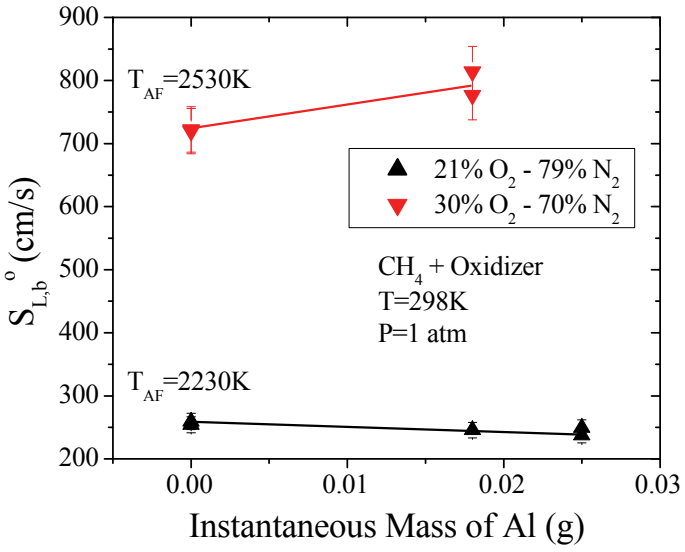

Figure 34 Burning velocity results for hybrid mixtures of Al nano-particles and stoichiometric Methane with different ratios of O_2:N_2 in the oxidizer. The lines are intended to serve as a visual aid.

Table 3 Experimental data for hybrid mixture of $Al/CH_4/O_2/N_2$ used in the direct injection experiments.

Mass Loading of Aluminum (g)	Instantaneous Mass of Aluminum (g)	Burned Gas Velocity, $S_{L,b}^{o}$ (cm/s)	
		21% O_2 – 79% N_2	30% O_2 – 70% N_2
0.00	0.00	254.0	722.3
0.00	0.00	259.3	719.8
0.25	0.018	245.7	814.2
0.25	0.018	-	776.6
0.35	0.025	237.3	-
0.35	0.025	249.4	-

A period of approximately 4 minutes was provided between dispersion and ignition to allow the induced turbulence within the vessel to decay. During this time, the larger particles characteristically settle to the bottom of the vessel, but the smaller particles remain in suspension suggesting the presence of a monodisperse particle sample. The burned, un-stretched flame velocity ($S_{L,b}^{o}$) is plotted as a function of aluminum mass loading for each oxidizer mixture with methane in the figure. The lines in this figure are provided as a visual aid to show the relative trends. Based on other experiments using the same equipment to measure flame speeds, the uncertainty in the measurements are roughly 5-10%. A distinct difference was observed for each ratio of O_2:N_2 in the oxidizing mixture when aluminum particles were added. For the experiments performed with stoichiometric methane-air (21:79 O_2:N_2), the burned gas velocity decreased as the amount of aluminum increased. This result is likely due to the aluminum absorbing a portion of the heat of combustion, reducing temperature and thus reaction rate. It is worthy to note after each experiment with 21% O_2-79% N_2, unburned aluminum particles were present at the bottom of the vessel.

When the ratio of O_2:N_2 was changed to 30:70, the burning velocity increased by about 10% with an aluminum mass loading of 0.018 g. Inspection of the vessel after the experiments with this O_2:N_2 ratio strongly suggests most if not all the aluminum was consumed in the reaction. No particles were present at the bottom of the vessel. However, the inside wall of the vessel was uniformly coated with a very thin, grey film that wipes off easily. Dynamic pressure data were also obtained for the experiments conducted

with 30:70-O_2:N_2 for the different aluminum mass loadings and is plotted in Figure 35. A difference is seen for a mass loading of 0.018 g of aluminum compared to 0.00 g. The two pressure traces for each mass loading that is presented indicate a certain degree of repeatability associated with the direct injection approach.

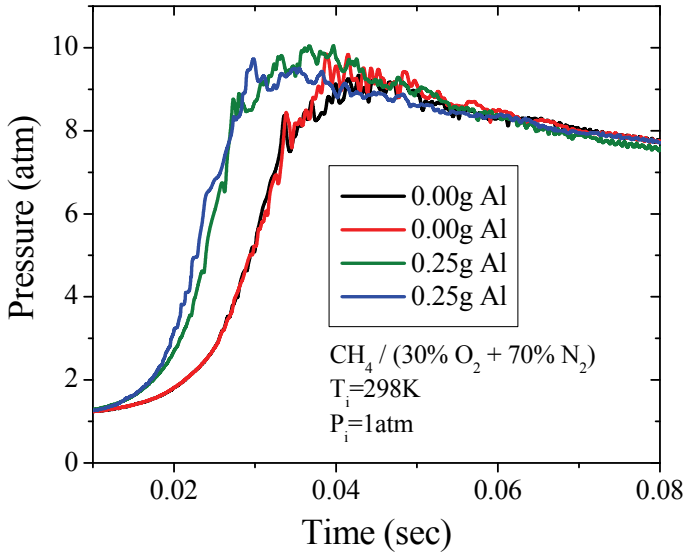

Figure 35 Dynamic pressure data for four experiments performed with and without aluminum nanoparticles. Mass of Al represents the original mass loading in the injector; the actual aerosol mass loading during the experiment was 0.018 g.

Figure 36 provides a closer view of the pressure traces from both aluminum mass loadings. It is seen in this figure that the 0.25-g experiment experiences a much higher rate of change of pressure (*dP/dt*) compared to the 0.00-g counterpart. The 0.25-g experiment reached the peak pressure in 0.035 seconds, yielding a *dP/dt* of approximately 290 atm/sec. Without aluminum, the maximum pressure is achieved over a time period of 0.045 seconds, resulting in a *dP/dt* of approximately 200 atm/sec. In addition, a higher peak pressure was recorded for the 0.25-g aluminum case. The pressure data provided in these figures strongly suggest that the aluminum particles were participating in the overall combustion process.

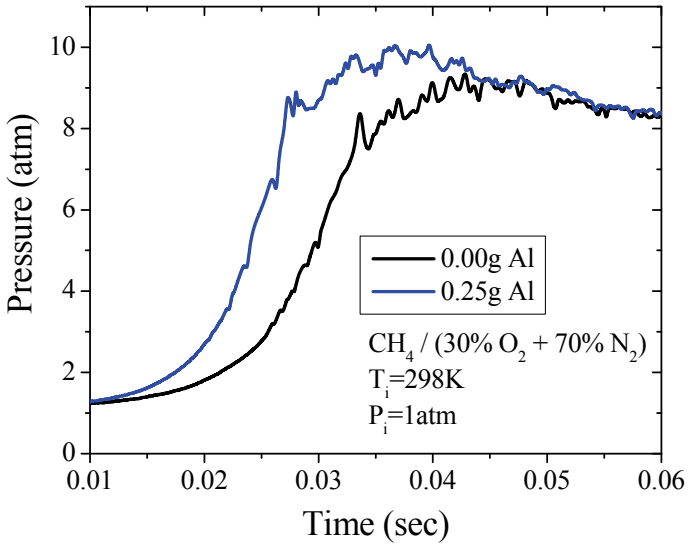

Figure 36 Close-up of dynamic pressure response for different mass loadings of Aluminum powder. Mass of Al represents the original mass loading in the injector; the actual aerosol mass loading during the experiment was 0.018 g.

Sample images from these conditions are also shown for comparison in Figure 37. The images presented for both experiments with 0.25 grams of nano-Al particle directly injected into the aluminum flame speed vessel are optically transparent enough to visualize with the optical system and distinguish the flame edge using the post-processing script. Even though particles were dispersed with a strong blast of air, enough time was given for the turbulence to decay, as indicated in the smooth, spherical shape of the flames. For the same aluminum mass loading, and O_2:N_2-30:70, the flame developed small-scale cellular structures at larger flame radii. Despite these noticeable morphological features, the flame ball was still spherical in shape throughout the propagation regime. Post processing of the images further confirmed that flames did not accelerate and remained laminar throughout the tests (Lowry et al., 2011).

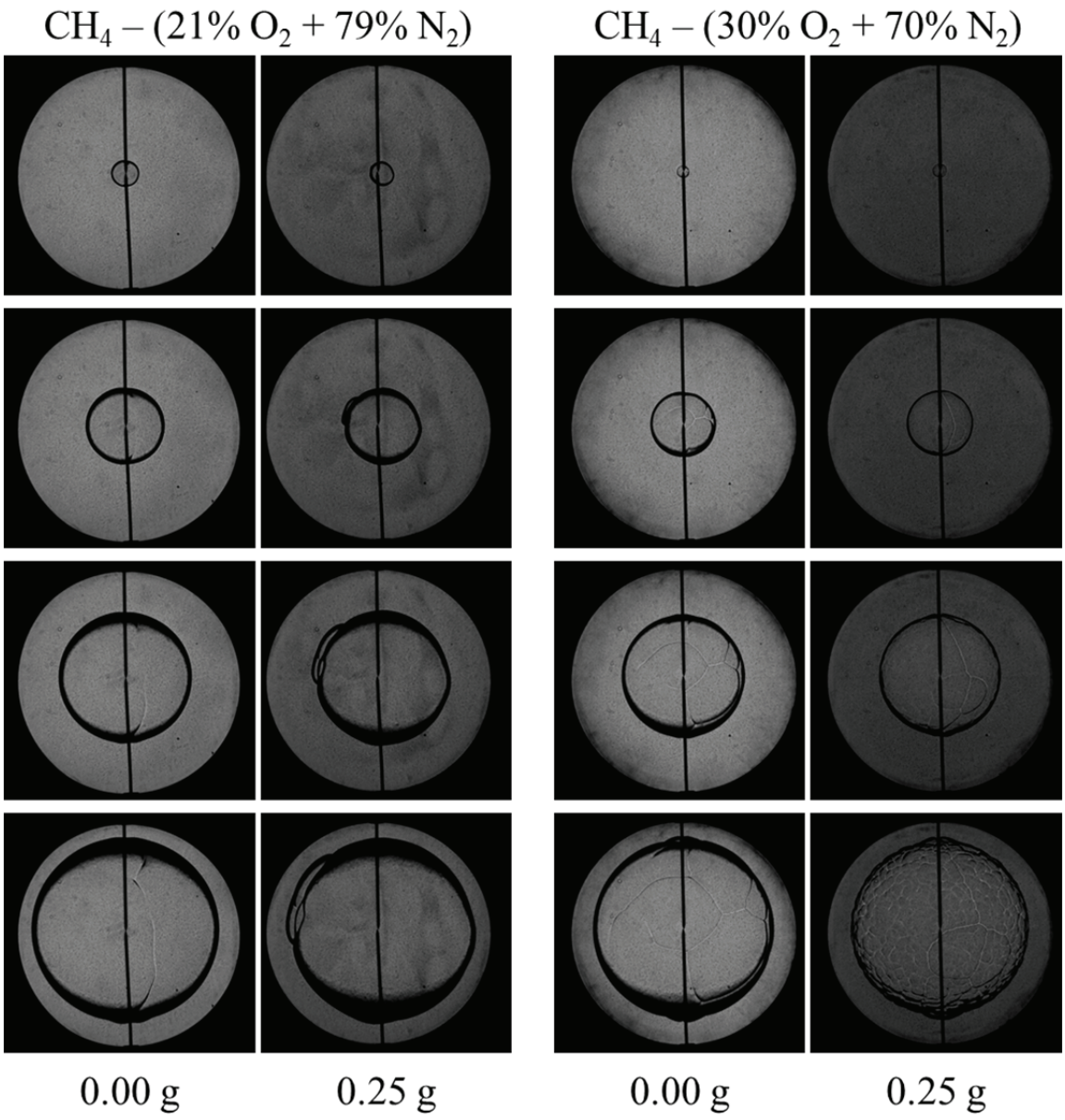

Figure 37 Experimental images of hybrid mixtures of $Al/CH_4/O_2/N_2$. Each column represents one experiment. Mass loading of Aluminum particles for each experiment is noted at the bottom of each column.

CHAPTER V

CONCLUSIONS AND SUGGESTIONS

This thesis provided an overview of the steps taken to develop an experimental facility for flame speed measurements in powdered aerosols. Using a previously developed particle dispersion technique, heterogeneous mixtures were created in a side vessel and transported into the main experimental facility. Combustion experiments were performed in a constant-volume, cylindrical vessel with optical access at each end, and flame propagation was recorded as a function of time. A Z-type schlieren setup was used in conjunction with a high-speed camera to record the spherically expanding flame front. The time-dependent area of the flame was compensated for flame stretch using a linear relationship between the flame stretch and the burned flame speed.

Two methods for introducing the nano-aluminum particles in a controlled, turbulent-free environment were tested—one involving the transfer of the aerosol from a side vessel, the other using a direct injection approach. Using the proposed "side-vessel" methodology, initial experiments were performed using a hybrid mixture of CH_4-(30:70 O_2:N_2) and nano-Al particles. Extinction diagnostics were completed on both the PVC-AMV and the aluminum flame speed vessel to characterize the injection and transfer processes. The extinction measurement within the flame speed vessel detected the presence of particles, but the actual number density was relatively small. This low loading is also reflected in the experimental results of the transfer method, where little change in the flame speed and pressure rise was detected.

The second, direct-injection approach provided a higher, more repeatable mass loading of particles and was therefore used to validate the system sensitivity to the presence of nano-Al particles for different nitrogen dilution ratios within the hybrid mixture of Al/CH_4/O_2/N_2. Flame images and dynamic pressure data were obtained for these experiments and suggest the aluminum particles do not burn when air is used as the oxidizer. This negligible impact is attributed to the flame temperature being below the melting point of the Al_2O_3 layer surrounding each particle. When the ratio of O_2:N_2 is changed to 30:70,

the flame temperature is raised above the Al_2O_3 melting point, and as a result changes in the combustion behavior of the hybrid mixture were detected when aluminum particles were present. In addition, the flame images indicate laminar conditions are present within the vessel using the direct-injection technique. This favorable finding is because a period of 4 minutes was given between dispersion and ignition for the induced turbulence within the vessel to decay.

Future work involves additional improvement to the experimental "transfer" methodology. Initial results with this method show a strong dependence on the force at which the aerosol is injected, and a more repeatable process is sought. Further exploration of the effect of wait times on the burning velocity and pressure rise within the vessel is also required. The simplicity of the direct-injection technique compared to the side-vessel methodology is desirable and will be further investigated as a viable alternative, or improvement, to the side-vessel technology. In other words, a repeatable aerosol can be produced in the side chamber using a direct-injection technique rather than the cumbersome piston-injector used in this thesis. In addition, the experimental flame speed data can be used to develop a mathematical model of flame propagation in powdered aerosols.

REFERENCES

Amyotte, P.R. and Pegg, M.J. 1989. Lycopodium dust explosions in a Hartmann bomb: effects of turbulence. *Journal of Loss Prevention in the Process Industries*, **2**, 87-94.

ASTM Standard. 2007a. *Standard Test Method for Minimum Explosible Concentration of Combustible Dusts*. E1515-07.

ASTM Standard. 2007b. *Standard Test Method for Minimum Ignition Energy of a Dust Cloud in Air*. E2019-03.

ASTM Standard. 2010. *Standard Test Method for Explosibility of Dust Clouds*. E1226-10.

Badin, E.J., Stuart, J.G., and Pease, R.N. 1949. Burning velocities of butadiene-1, 3 with nitrogen-oxygen and helium-oxygen mixtures. *Journal of Chemical Physics*, **17**, 314-316.

Bohren, C.F., and Huffman, D.R. 1998. *Absorption and Scattering of Light by Small Particles*, Wiley, New York.

Bradley, D., Chen, Z., and Swithenbank, J.R. 1988. Burning rates in turbulent fine dust-air explosions. *Symposium (International) on Combustion*, **22**, 1767-1775.

Bradley, D., and Mitcheson, A. 1976. Mathematical solutions for explosions in spherical vessels. *Combustion and Flame*, **26**, 201-217.

Brown, M.J., McLean, I.C., Smith, D.B., and Taylor, S.C. 1996. Markstein lengths of CO/H_2/air flames, using expanding spherical flames. *Proceedings of the Combustion Institute*, **26**, 875-881.

Cashdollar, K.L. 2000. Overview of dust explosibility characteristics. *Journal of Loss Prevention in the Process Industries*, **13**, 183-199.

Cashdollar, K.L., and Chatrathi, K. 1992. Minimum explosible dust concentrations measured in 20-l and 1-m^3 chambers. *Combustion Science and Technology*, **87**, 157-171.

Cashdollar, K.L., Zlochower, I.A. 2007. Explosion temperatures and pressures of metals and other elemental dust clouds. *Journal of Loss Prevention in the Process Industries*, **20**, 337-348.

CHEMKIN. 2008. Reaction Design, San Diego, CA.

Chowdhury, M.H., Ray, K., Gray, S.K., Pond, J., and Lakowicz, J.R. 2009. Aluminum nanoparticles as substrates for metal-enhanced fluorescence in the ultraviolet for the label-free detection of biomolecules. *Analytical Chemistry*, **81**, 1397-1403.

Clingman, W.H., Brokaw, R.S., and Pease, R.N. 1953. Burning velocities of methane with nitrogen-oxygen, argon-oxygen, and helium-oxygen mixtures. *Proceedings of the Combustion Institute*, **4**, 310-313.

Continillo, G., Crescitelli, S., Fumo, E. Napolitano, F., and Russo, G. 1991. Coal dust explosions in a spherical bomb. *Journal of Loss Prevention in the Process Industries*, **4**, 223-229.

Dahoe, A.E., Cant, R.S., Pegg, M.J., Scarlett, B., 2001. On the transient flow in the 20-liter explosion sphere. *Journal of Loss Prevention in the Process Industries*, **14**, 475-487.

Dahoe, A.E., Hanjalic, K., Scarlett, B. 2002. Determination of the laminar burning velocity and the Markstein length of powder-air flames. *Powder Technology*, **122**, 222-238.

Dahoe, A.E., van Velzen, Th.J., Sluijs, L.P., Neervoort, F.J., Leschonski, S., Lemkowitz, S.M., van der Wel, P.G.J., and Scarlett, B. 1995. Construction and operation of a 20-litre dust explosion sphere at and above atmospheric conditions. *Journal of Loss Prevention and Safety Promotion in the Process Industries*, **2**, 285-302.

Dahoe, A.E., Zevenbergen, J.F., Lemkowitz, S.M., and Scarlett, B. 1996. Dust explosions in spherical vessels: The role of flame thickness in the validity of the 'cube-root law'. *Journal of Loss Prevention in the Process Industries*, **9**, 33-44.

Dastidar, A.G., Nalda-Reyes, B., and Dahn, C.J. 2005. Evaluation of dust and hybrid mixture explosion potential in process plants. *Process Safety Progress*, **24**, 294-298.

de Vries, J. 2009. *A study on spherical expanding flame speeds of methane, ethane, and methane/ethane mixtures at elevated pressures*, PhD dissertation, Texas A&M University, College Station, TX, USA.

Dowdy, D.R., Smith, D.B., Taylor, S.C., and Williams, A. 1990. The use of expanding spherical flames to determine burning velocities and stretch effects in hydrogen/air mixtures. *Proceedings of the Combustion Institute*, **23**, 325-332.

Dufaud, O., Traore, M., Perrin, L., Chazelet, S., Thomas, D. 2010. Experimental investigation and modeling of aluminum dusts explosions in the 20 l sphere. *Journal of Loss Prevention in the Process Industries*, **23**, 226-236.

Eckhoff, R.K. 2003. *Dust Explosions in the Process Industries*, 3rd ed., Gulf Professional Publishing/Elsevier, Boston.

Escot Bocanegra, P., Davidenko, D., Sarou-Kanian, V., Chauveau, C., and Gokalp, I. 2010. Experimental and numerical studies on the burning of aluminum micro and nanoparticle clouds in air. *Experimental Thermal and Fluid Science*, **34**, 299-307.

Gibbs, G.J. and Calcote, H.F. 1959. Effect of molecular structure on burning velocity. *Journal of Chemical and Engineering Data*, **4**, 226-237.

Goroshin, S., Fomenko, I., and Lee, J.H.S. 1996. Burning velocities in fuel-rich aluminum dust clouds. *Symposium (International) on Combustion*, **26**, 1961-1967.

Hertzberg, M., Zlochower, A., and Cashdollar, K.L. 1992. Metal dust combustion: explosion, limits, pressures, and temperatures. *Symposium (International) on Combustion*, **24**, 1827-1835.

Hinds, W.C. 1999. *Aerosol Technology: Properties, Behavior, and Measurement of Airborne Particles*, 2nd ed. John Wiley & Sons, Inc. New Jersey.

Huang, Y., Risha, G.A., Yang, V., and Yetter, R.A. 2009. Effect of particle size on combustion of aluminum particle dust in air. *Combustion and Flame*, **156**, 5-13.

International Standards Organization (ISO). 1985. *Explosion Protection Systems – Part 1: Determination of Explosion Indices of Combustible Dusts in Air*, ISO 6184-1.

Kalitan, D.M. and Petersen, E.L. 2007. Nano-aluminum aerosol characterization with application to heterogeneous shock-tube combustion. *Presented at the 5th US Combustion Meeting*, Paper # D18.

Kalitan, D.M., Petersen, E.L., and Crofton, M.W. 2006. A shock-tube study of aluminum oxidation at elevated temperatures. AIAA/ASME/SAE/ASEE Joint Propulsion Conference and Exhibit, **42**, AIAA 2006-4405.

Krause, U., and Kasch, T. 2000. The influence of flow and turbulence on flame propagation through dust-air mixtures. *Journal of Loss Prevention in the Process Industries*, **13**, 291-298.

Law, C.K. 2006. *Combustion Physics*, 1st ed. Cambridge University Press, New York.

Liebhafsky, H.A. and Pfeiffer, H.G. 1953. Beer's law in analytical chemistry. *Journal of Chemical Education*, **30**, 450-452.

Lin, B.-Q., Li, W.-X., Zhu, Ch.-J., Lu, H.-L., Lu, Zh.-G., and Li, Q.-Zh. 2010. Experimental investigation on explosion characteristics of nano-aluminum powder-air mixtures. *Combustion, Explosion, and Shock Waves*, **46**, 678-682.

Lowry, W., de Vries, J., Krejci, M., Serinyel. Z., Metcalfe, W., Curran, H., Petersen, E., and Bourque, G. 2011. Laminar flame speed measurements and modeling of pure alkanes and alkane blends at elevated pressures. *Journal of Engineering for Gas Turbines and Power*, **133**, 091501.

Luijten, C.C.M., Doosje, E., van Oijen, J.A., de Goey, L.P.H. 2009. Impact of dissociation and end pressure on determination of laminar burning velocities in constant volume combustion, **48**, 1206-1212.

Malinin, D.R. and Yoe, J.H. 1961. Development of the laws of calorimetry. *Journal of Chemical Education*, **38**, 129-131.

Markstein, G.H. 1964. *Non-Steady Flame Propagation*, Pergamon, New York.

National Fire Protection Association (NFPA) 654. 2000. *Standard for the prevention of fire and dust explosions from the manufacturing, processing, and handling of combustible particulate solids*, *2000 Edition.* NFPA, Quincy, MA.

Parker, T.E., Foutter, R.R., and Rawlins, W.T. 2001. A pulsed particle injection system for shock tube studies of powders. *Review of Scientific Instruments*, **72**, 263-267.

Peng, Y., Wang, Y., Yang, Y. and Dlott, D.D. 2009. Simulation of the absorption spectra of nanometallic Al particles with core-shell structure: size-dependent interband transitions. *Journal of Nanoparticle Research*, **12**, 777-787.

Pfeiffer, H.G. and Liebhafsky, H.A. 1951. The origins of Beer's law. *Journal of Chemical Education*, 123-125.

Proust, C. 2006a. A few fundamental aspects about ignition and flame propagation in dust clouds. *Journal of Loss Prevention in the Process Industries*, **19**, 104-120.

Proust, C. 2006b. Flame propagation and combustion in some dust-air mixtures. *Journal of Loss Prevention in the Process Industries*, **19**, 89-100.

Proust, C., and Veyssiere, B. 1988. Fundamental properties of flames propagating in starch dust-air mixtures. *Combustion Science and Technology*, **62**, 149-172.

Pu, Y.K., Jarosinski, J., Johnson, V.G., and Kauffman, C.W. 1990. Turbulence effects on dust explosions in the 20-liter spherical vessel. *Symposium (International) on Combustion*, **23**, 843-849.

Pu, Y.K., Jia, F., Wang, S.F., and Skjold, T. 2007. Determination of the maximum effective burning velocity of dust-air mixtures in constant volume combustion. *Journal of Loss Prevention in the Process Industries*, **20**, 462-469.

Quinten, M. 2011. *Optical Properties of Nanoparticle Systems*, Wiley-VCH, Weinheim, Germany.

Santhanam, P.R., Hoffmann, V.K., Trunov, M.A., and Dreizin, E.L. 2010. Characteristics of aluminum combustion obtained from constant-volume explosion experiments. *Combustion Science and Technology*, **182**, 904-921.

Settles, G.S. 2006. *Schlieren and shadowgraph techniques: visualizing phenomena in transparent media*, Springer, Heidelberg, Germany.

Signorell, R., and Reid, J.P. 2011. *Fundamentals and Applications in Aerosol Spectroscopy*, CRC Press, Florida.

Soundararajan, R., Amyotte, P.R., and Pegg, M.J. 1996. Explosibility hazard of iron sulphide dusts as a function of particle size. *Journal of Hazardous Materials*, **51**, 225-239.

Swinehart, D.F. 1962. The Beer-Lambert law. *Journal of Chemical Education*, **39**, 333-335.

Temple, T.L., and Bagnall, D.M. 2011. Optical properties of gold and aluminum nanoparticles for silicon solar cell applications. *Journal of Applied Physics*, **109**, 084343.

U.S. Chemical Safety and Hazard Investigation Board (U.S. CSB). 2009. *Investigation report. Sugar dust explosion and fire, Imperial Sugar Company*, Report No. 2008-05-I-GA.

U.S. CSB. 2006. *Combustible dust hazard study*, Report No. 2006-H-1.

U.S. CSB. 2004. *Investigation report. Dust explosion, West Pharmaceutical Services, Inc.*, Report No. 2003-07-I-NC.

Veyssiere, B. 1992. Development and propagation regimes of dust explosions. *Powder Technology*, **71**, 171-180.

Wang, S., Pu, Y., Jia, F., Gutkowski, A., and Jarosinski, J. 2006. An experimental study on flame propagation in cornstarch dust clouds. *Journal of Combustion Science and Technology*, **178**, 1957-1975.

Zhen, G. and Leuckel, W. 1997. Effect of ignitors and turbulence on dust explosions. *Journal of Loss Prevention in the Process Industries*, **10**, 317-324.

APPENDIX

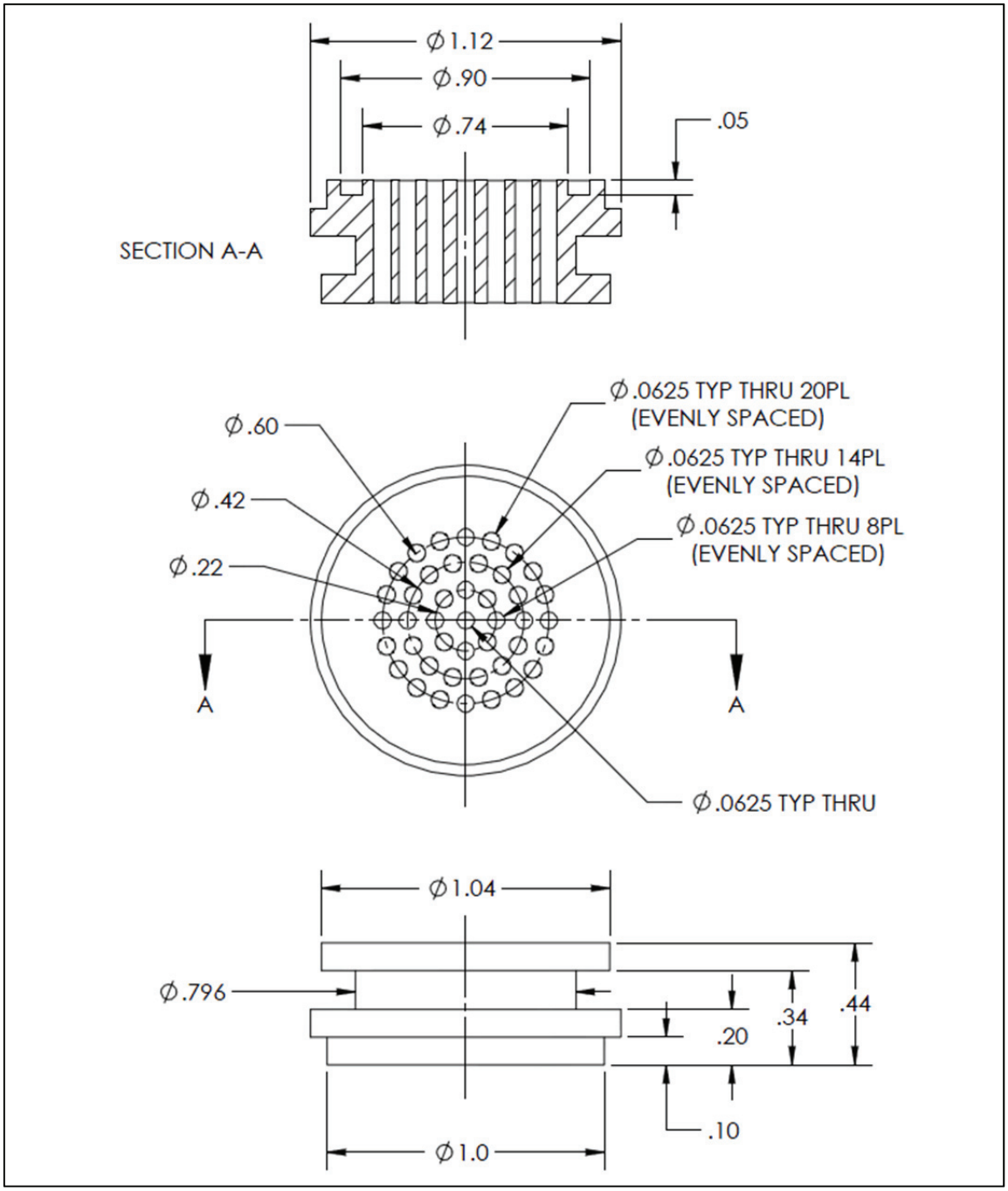

Figure A1 Detailed drawing of Flow Splitting Plate.

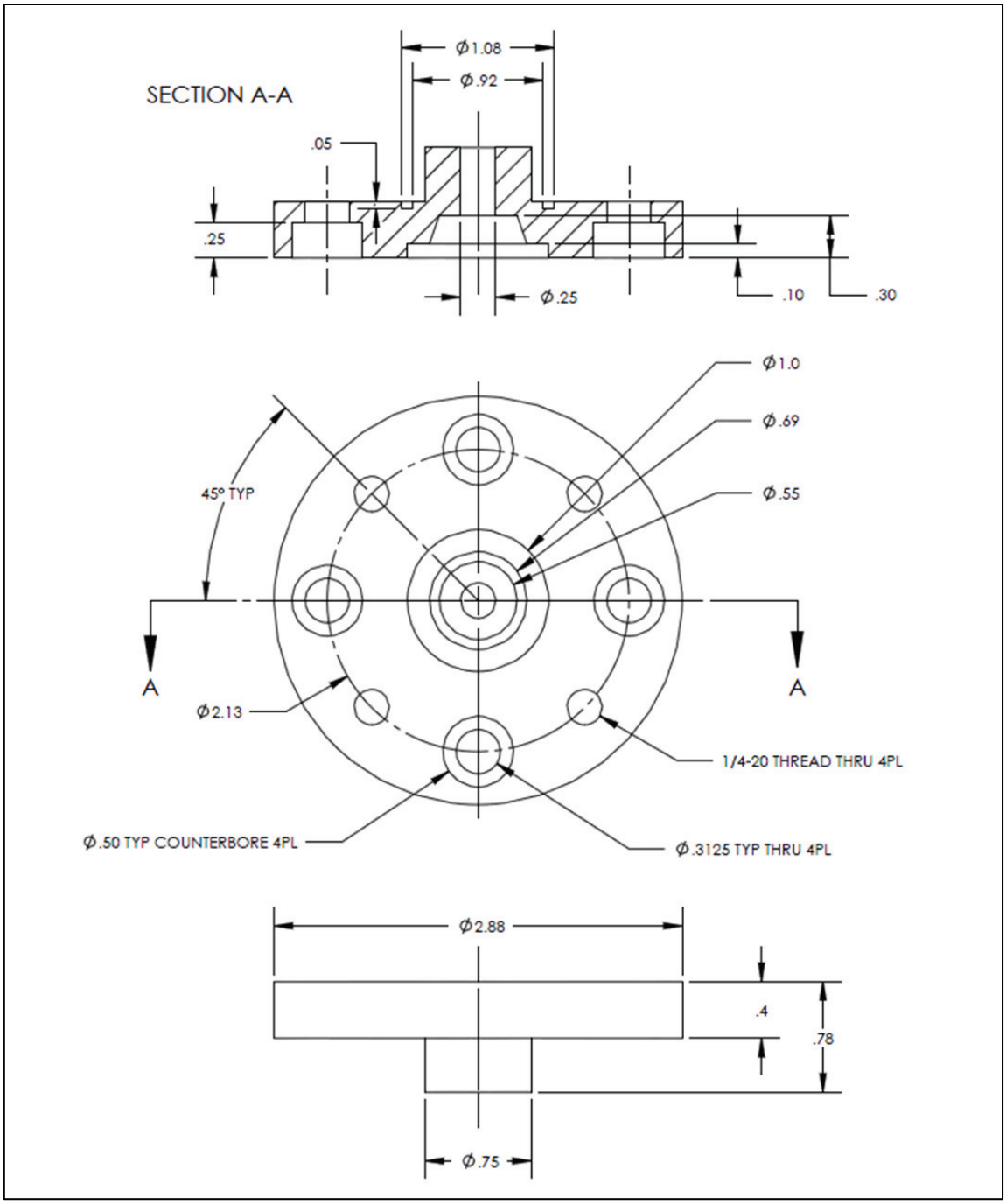

Figure A2 Detailed drawing of Nozzle Section.

VITA

Andrew John Vissotski received his Bachelor of Science degree in mechanical engineering from Boise State University in May 2010. He then entered the graduate program at Texas A&M University and received his Master of Science degree in mechanical engineering in August 2012. During his graduate work, Vissotski co-authored 1 journal publication and 4 conference papers, and authored 1 conference paper. He also gave presentations at the Spring Technical Meeting of the Central States Section of the Combustion Institute and at the Steering Committee Meeting of the Mary Kay O'Connor Process Safety Center at Texas A&M. His interests include combustion science, gas dynamics, thermodynamics, propulsion systems, and engineering design.

Mr. Vissotski may be reached at the Department of Mechanical Engineering, 3123 TAMU, Texas A&M University, College Station, TX 77843-3123. His email address is andrewvissotski@gmail.com.